NASA TECHNICAL NOTE

NASA TN D-2907

EXPERIMENTAL INVESTIGATION OF A TURBULENT BOUNDARY LAYER AT MACH 6, HIGH REYNOLDS NUMBERS, AND ZERO HEAT TRANSFER

by Jerry B. Adcock, John B. Peterson, Jr., and Donald I. McRee

Langley Research Center
Langley Station, Hampton, Va.

NATIONAL AERONAUTICS AND SPACE ADMINISTRATION • WASHINGTON, D. C. • JULY 1965

NASA TN D-2907

EXPERIMENTAL INVESTIGATION OF A TURBULENT BOUNDARY LAYER AT MACH 6, HIGH REYNOLDS NUMBERS, AND ZERO HEAT TRANSFER

By Jerry B. Adcock, John B. Peterson, Jr., and Donald I. McRee

Langley Research Center
Langley Station, Hampton, Va.

NATIONAL AERONAUTICS AND SPACE ADMINISTRATION

For sale by the Clearinghouse for Federal Scientific and Technical Information
Springfield, Virginia 22151 – Price $3.00

EXPERIMENTAL INVESTIGATION OF A TURBULENT BOUNDARY LAYER AT MACH 6, HIGH REYNOLDS NUMBERS, AND ZERO HEAT TRANSFER

By Jerry B. Adcock, John B. Peterson, Jr.,
and Donald I. McRee
Langley Research Center

SUMMARY

29843

An experimental investigation of the turbulent boundary layer on a hollow cylinder was made at a Mach number of 6 and with adiabatic wall temperature at Reynolds numbers based on the distance from the leading edge from 5×10^6 to 33×10^6. Data obtained include turbulent recovery factors, a total temperature profile, velocity profiles, and average skin-friction coefficients by the momentum method.

The turbulent recovery factor was found to be approximately 0.88; a slight decrease of recovery factor with increase in Reynolds number was obtained. The velocity profiles, when compared with power profiles, were found to have an increasing exponent with increasing Reynolds number. The measured temperatures in the boundary layer were compared with two theoretical temperature distributions, the Crocco laminar distributions used by Van Driest (NACA TN 2597), a quadratic distribution used by Donaldson (NACA RM L52H04), and with the assumption of a constant total temperature through the boundary layer. The assumption of a constant total temperature was found to give the most accurate value of momentum thickness. The skin-friction results were compared with the theories of Van Driest, Wilson and Van Driest, Cope and Monaghan, with the Sommer and Short T' method, and also with other experimental data.

Author

INTRODUCTION

Since turbulent boundary layers will exist on large portions of the surface of high-speed vehicles, it is essential to know their characteristics. Turbulent boundary layers, however, are not as amenable to theory as laminar boundary layers; therefore, experimental determination of their characteristics must be made in order to check the validity of the various theories. In turbulent flow there is wide variation in the many theories. This variation can be seen in figure 1 of reference 1, in which the large difference in values predicted by the various skin-friction theories is shown. Many correlations of the skin-friction theories and the available experimental data have been made. One of

the latest correlations can be found in reference 2. It should be noted, however, that most of the data were obtained at the lower Mach numbers and Reynolds numbers and that the differences in the skin-friction theories become greater at the higher Mach numbers.

The purpose of this investigation was to provide turbulent-boundary-layer data at a hypersonic Mach number of 6 and high Reynolds numbers based on the distance from the leading edge (5×10^6 to 33×10^6). Turbulent-boundary-layer velocity profiles were obtained from pitot-pressure surveys through the boundary layer on a hollow cylinder. These velocity profiles are compared with theoretical power profiles. Average skin-friction coefficients were obtained by use of the momentum method. In this method the momentum thickness is calculated from a pitot-pressure survey and from a temperature distribution through the boundary layer. Normally, at low Mach numbers the assumption of a constant total temperature through the boundary layer is made. In order that a better insight into the temperature distribution which should be used at a Mach number of 6 be gained, a total-temperature survey was made.

In addition to the skin-friction coefficients and velocity profiles calculated from the temperature and pitot-pressure survey data, turbulent recovery factors were also obtained from wall-temperature measurements.

The present skin-friction coefficients, along with other authors' experimental skin-friction data, are compared with four of the well-known theories: Sommer and Short (ref. 3), Van Driest (ref. 4), Wilson (ref. 5 or 6) and Van Driest (ref. 7), Cope (ref. 8), and Monaghan and Johnson (ref. 9).

SYMBOLS

$A,B,C,D,K,$ a,b,c	constants
C_F	average skin-friction coefficient
C_f	local skin-friction coefficient
c_p	specific heat at constant pressure
i	limits of summation
M	Mach number
$\bar{M}_\delta$	Mach number in constant-pressure plane (average Mach number at edge of boundary layer)
n	exponent in power-profile relation, $\frac{u}{U_\delta} = \left(\frac{y}{\delta}\right)^{1/n}$

p	pressure
p'	pitot pressure
R	Reynolds number per foot
R_{le}	Reynolds number based on distance from leading edge of model
R_{le-x}	Reynolds number based on distance from leading edge to virtual origin of turbulent boundary layer
R_x	Reynolds number based on distance from virtual origin of turbulent boundary layer
R_θ	Reynolds number based on boundary-layer momentum thickness
$R_{\bar{\theta}}$	Reynolds number based on $\bar{\theta}$
r	radius of cylinder, 3 inches
T	temperature
T_t	total temperature
U_δ	velocity at outer edge of boundary layer
u	velocity in boundary layer
x	distance from virtual origin of turbulent boundary layer
x_{le}	distance from leading edge of model
y	distance, or height, normal to model, measured from surface
α	angle of attack
γ	ratio of specific heats
δ	boundary-layer thickness
δ_{pr}	boundary-layer thickness based on pitot-pressure profile
δ^*	boundary-layer displacement thickness (see eq. (9))
δ^*/θ	boundary-layer shape factor
η	recovery factor
θ	momentum thickness of boundary layer (see eq. (8))

$\bar{\theta}$	momentum thickness based on Mach number in plane of constant pressure (see eq. (10))
θ_H	boundary-layer total-enthalpy thickness (see eq. (3))
θ^I, θ^{II}	coefficients used in equation (6)
ρ	gas density
ψ	angle of yaw

Subscripts:

aw	adiabatic wall
i	incompressible
max	maximum
p	measured by boundary-layer probe
t	total or stagnation conditions
w	wall or wall conditions
δ	conditions at edge of boundary layer

APPARATUS

Wind Tunnel

The tests were conducted in the Langley 20-inch Mach 6 tunnel. This tunnel is of the blowdown type; however, the capacity of the air-supply pumps was large enough to allow test runs as long as 45 minutes in this investigation. The tunnel has a rectangular test section 20 inches by 20.5 inches. Maximum operating stagnation pressure is about 525 psia and maximum stagnation temperature is about 600° F. A schematic drawing and further information can be found in reference 10.

Model

The hollow-cylinder model used in the test is shown schematically in figure 1. The model outside diameter is 6 inches for a length of 42 inches and then flares out at an angle of 20° to a diameter of 8 inches. This larger diameter was needed to facilitate the circulation of a coolant between the inside and outside walls of the model for further cooled-wall boundary-layer investigation. The leading edge was beveled inward at an angle of 15° until the inside diameter of the model was 5 inches.

Located at 1.15 inches behind the leading edge was a transition trip used to cause early transition. This transition trip was made of 0.075-inch-diameter steel rods mounted normal to the surface by pressing them into drilled holes. The trip was made with the rods spaced every 0.25 inch around the circumference of the model with an original height of 0.075 inch. A preliminary study using fluorescent-oil-flow visualization, however, showed separation occurring just ahead of the transition trip. Therefore, the height of the trip was ground off in progressive steps until no separation was apparent. The trip height was 0.025 inch when no separation occurred, and it was this height that was used for the results presented herein. A photograph of the leading-edge ring with the trip is shown in figure 2.

Instrumentation

Static-pressure orifices were located circumferentially on the cylinder, 90° apart, at each of the 18-, 26-, and 34-inch stations (measured from the leading edge). There was also another orifice located 10 inches from the leading edge. (See fig. 1.) The static pressures were measured with a Statham pressure transducer (range from 0 to 1 psia), mounted on an electrically actuated pressure scanning valve so that all the static orifices were read by the same transducer. This arrangement allowed a more accurate comparison to be made of the static pressures at various positions on the model.

The pitot pressures obtained during the boundary-layer survey were measured by three Statham pressure transducers manifolded together and connected to another electrically actuated pressure scanning valve. The three transducers had the following ranges: from 0 to 1 psia, from 0 to 5 psia, and from 0 to 15 psia. This arrangement provided increased accuracy by permitting the pressure measurements to be taken from the gage which was nearest full-scale reading. A zero reading was taken on all pressure transducers before each run by using a reference pressure.

Five swaged copper-constantan thermocouples were spot welded to the inside surface of the 0.12-inch-thick outside wall of the model at distances of 6, 14, 22, 30, and 38 inches from the leading edge. The thermocouples were referenced to an insulated junction box outside the tunnel. The temperature of the insulated junction box was read on a 12-channel recording potentiometer. All the thermocouple and pressure-transducer outputs were recorded on a high-speed analog to digital data recording system.

Probes and Survey Apparatus

Schematics of the boundary-layer total-pressure and total-temperature survey probes used in the tests are shown in figures 3 and 4, respectively. The pressure probe had an outside diameter of 0.050 inch and was made of stainless-steel tubing flattened to a height of 0.007 inch with an opening height of 0.003 inch at the tip. This tube was silver soldered into progressively larger tubing leading to the tubing (0.25-inch outside diameter) which formed the vertical shaft of the probe.

The temperature probe was made from a swaged thermocouple with a 0.014-inch outside diameter. The end of the swaged thermocouple was flared to approximately 0.020-inch diameter and two 0.007-inch-diameter holes were drilled in the side wall for exits. The thermocouple was of 0.001-inch-diameter chromel-alumel wires, and the reference junction was placed in an ice bath outside the tunnel.

The probe survey mechanism was driven by an electric motor and could position the survey probe in the boundary layer with an accuracy of ±0.0005 inch. The probe was electrically insulated from ground, and the position of the model surface was indicated by electrical contact of the probe with the model after equilibrium conditions were established in the tunnel. The survey mechanism also allowed the probe to be moved 10 inches in the streamwise direction while the tunnel was in operation so that various stations on the model could be surveyed.

TESTS

The tests were conducted at a free-stream Mach number of 6. The Reynolds number per foot was approximately 10×10^6 obtained with a tunnel stagnation pressure of 525 psia and a stagnation temperature of 415° F ± 10° F. In order for the model wall to reach equilibrium temperature, the tunnel was operated for approximately 10 minutes before boundary-layer measurements were made. Total-pressure surveys of the boundary layer were made at seven different stations (however, two surveys were made at the 40-inch station). These stations were along the top of the model at distances of 5, 6, 8, 11, 33, 37, and 40 inches from the leading edge. In addition to the total-pressure surveys, a total-temperature survey of the boundary layer was made at the 33-inch station. Surface temperatures and static pressures were measured during each survey. Schlieren photographs were taken in order to show the boundary-layer development for both natural and artificially produced transition.

At the initiation of the test program, the model had to be alined with the stream flow. Figure 5(a) gives the static-pressure distribution around the model with the initial alinement. Also included in the figure are the angles of attack and yaw calculated from two-dimensional theory. Figure 5(b) gives the same information after final alinement. The angle of attack calculated from the latter distribution was less than -0.05° and the angle of yaw was less than 0.10°.

RESULTS AND DISCUSSION

Turbulent Recovery Factors

With the five thermocouples, wall temperatures were measured at various distances from the leading edge. The recovery factors were calculated from these measurements in order to check the validity of the assumption of zero

heat transfer. The recovery factors are defined by

$$\eta = \frac{T_w - T_\delta}{T_{t,\delta} - T_\delta} \tag{1}$$

and are plotted against x_{le} in figure 6. The quantity T_δ is the local static temperature at the edge of the boundary layer at any particular station. The average value of the turbulent recovery factor is seen to be approximately 0.88.

The radiation effect on the wall temperature was theoretically determined at the maximum radiation condition which occurred on the part of the model surface that can be seen through the schlieren windows. (See fig. 1.) Here the effect was found to decrease the wall temperature approximately 4° and decrease the recovery factor about 0.5 percent. Since this effect was not significant, no attempt to correct the wall temperatures was made.

The plot in figure 6 shows a gradual decrease in recovery factor with distance from the leading edge. This decrease is also shown in references 11 and 12 for which the recovery factors were obtained at Mach numbers of 2.4 and from 0.87 to 5.05, respectively. At the low Reynolds numbers for which a comparison can be made, the recovery factors of the present test agree very well with those in reference 12 at a Mach number of 5.05.

Total-Temperature Profile

Total-temperature survey.- A total-temperature survey of the boundary layer as well as a pitot-pressure survey was made at the 33-inch station. The calibration of the temperature probe showing the variation of the probe recovery factor with Mach number and Reynolds number per foot was obtained from data taken in the Langley Unitary Plan wind tunnel at stagnation temperatures of 150° F and 230° F and is shown in figure 7. Also shown in the figure are the free-stream recovery factor obtained during the actual total-temperature survey and the interpolated curves necessary to go from the highest calibrated recovery factor to the free-stream recovery factor. The probe recovery factor is defined by

$$\eta_p = \frac{T_p - T}{T_t - T} \tag{2}$$

With this calibration and the Mach number and temperature-survey data at the 33-inch station (station 5; tables I and II), the total-temperature profile can be obtained by a quickly convergent iteration process of assuming a probe recovery factor η_p, finding the total temperature and Reynolds number from the assumed η_p, and then finding a new η_p with the Mach number and calculated Reynolds number. This process is repeated until the calculated η_p agrees with the assumed value. The final result of this iteration is shown in the

calibration plot (fig. 7) which gives the variation of Reynolds number with Mach number through the boundary layer. The total-temperature profile obtained in this way is shown in figure 8. As expected, several points in the boundary layer had total temperatures higher than the tunnel stagnation temperature.

An indication of the accuracy of the temperature measurements can be obtained by finding the boundary-layer total-enthalpy thickness. Theoretically, the total-enthalpy thickness θ_H should be zero for adiabatic wall conditions. The total-enthalpy thickness on a cylinder is defined as

$$\theta_H = \int_0^{\delta} \frac{\rho u}{\rho_\delta U_\delta}\left(\frac{T_t}{T_{t,\delta}} - 1\right)\frac{r + y}{r}\, dy \tag{3}$$

Figure 9 shows the integrand of equation (3) obtained from the pressure and temperature surveys at the 33-inch station and plotted against the height y. Good accuracy of the boundary-layer temperature probe is indicated inasmuch as the area under the curve, the total-enthalpy thickness θ_H, is virtually zero.

Comparison of measured temperatures with theory.- Since both a temperature and a pitot-pressure survey were made at the 33-inch station, a comparison of the measured temperature-velocity relationship with various assumptions for this relationship can be made. One assumption, commonly used at low Mach numbers, is that the total temperature is constant through the boundary layer. Another assumption which was used in reference 13 is that the temperature distribution through the boundary layer is similar to the Crocco quadratic form (ref. 14). This distribution is given by:

$$\frac{T}{T_\delta} = A\left(\frac{u}{U_\delta}\right)^2 + B\,\frac{u}{U_\delta} + D \tag{4}$$

where

$$A = 1 - \frac{T_{aw}}{T_\delta}$$

$$B = \frac{T_{aw}}{T_\delta} - \frac{T_w}{T_\delta} = 0 \qquad \text{(zero heat transfer)}$$

and

$$D = \frac{T_w}{T_\delta}$$

When equation (4) is transformed into its corresponding total-temperature distribution, it is seen to be of the form:

$$\frac{T_t}{T_{t,\delta}} = a\left(\frac{u}{U_\delta}\right)^2 + b\,\frac{u}{U_\delta} + c \qquad (5)$$

where

$$a = 1 - \frac{T_{aw}}{T_{t,\delta}}$$

$$b = \frac{T_{aw}}{T_{t,\delta}} - \frac{T_w}{T_{t,\delta}} = 0 \qquad \text{(zero heat transfer)}$$

and

$$c = \frac{T_w}{T_{t,\delta}}$$

Another assumption that might be made for the temperature-velocity relationship in a turbulent boundary layer is that it follows that of Crocco for the laminar boundary layer. This distribution is given by Van Driest in reference 14 and in the nomenclature of this report is

$$\frac{T_t}{T_{t,\delta}} = \frac{T_w}{T_{t,\delta}} - \left(\frac{T_w}{T_{t,\delta}} - \frac{T_\delta}{T_{t,\delta}}\right)\theta^I + \left(1 - \frac{T_\delta}{T_{t,\delta}}\right)\left[2\theta^{II} + \left(\frac{u}{U_\delta}\right)^2\right] \qquad (6)$$

where θ^I and θ^{II} are coefficients which are given in reference 14 and depend only on Prandtl number and velocity ratio u/U_δ. For use in this report a Prandtl number of 0.725 was assumed.

A plot of boundary-layer total-temperature ratio as a function of the velocity ratio squared is given in figure 10. This figure shows the quadratic and Crocco laminar distributions and the assumption of a constant total temperature, all compared with the measured total temperatures. It appears from this plot that the quadratic temperature distribution would more adequately match the measured distribution than would the assumption of a constant total temperature or the Crocco laminar distribution. This agreement is especially true in the inner portions of the boundary layer $\left(\text{i.e., for } \left(u/U_\delta\right)^2 < 0.7\right)$. However, a comparison in figure 11 of the momentum profiles at the 33-inch station using the measured temperature distribution and the theoretical distributions shows that the assumption of a constant total temperature gives a momentum thickness very close to the value obtained from the measured temperature, whereas the quadratic and Crocco laminar distributions give values that are 13 percent greater and 16 percent less, respectively.

A comparison of figures 10 and 11 indicates the necessity for a good theoretical turbulent temperature-velocity distribution to match closely the

temperature "bump" (that portion of the profile which exceeds the temperature $T_{t,\delta}$) in the outer portions of the boundary layer (fig. 10). The constant total temperature does not correspond with either the inner or outer portions; but when the momentum thickness is determined, the errors are compensating and give a reasonably accurate value for the momentum thickness. The quadratic distribution, though corresponding to the temperatures in the inner portion of the layer, fails to account for the high temperatures of the bump and, as a result, gives a value of momentum thickness that is too high. On the other hand, the Crocco laminar distribution predicts temperatures that are consistently too high for all parts of the turbulent boundary layer and gives a momentum thickness which is too low when compared with the momentum thickness of the measured distribution.

Reduction of the Pressure-Survey Data

In order to obtain the momentum thickness and velocity profile from the pitot-pressure survey, the temperature distribution must be known or a temperature-velocity relationship must be assumed. Since a total-temperature profile was measured only at the 33-inch station, it was necessary to assume a temperature-velocity relationship for the other survey stations. It was decided to use the temperature-velocity relationship obtained at the 33-inch station for the other stations also. It is realized that this relationship may be somewhat different at the other stations, but it seems certain that use of this particular temperature-velocity relationship should give more accurate velocity profiles than the commonly used assumption of a constant total temperature. As stated in the previous section, there was close agreement in the momentum thickness as determined by the two methods at the 33-inch station, but a comparison at the forward stations showed that they differ by as much as 5 percent. The method which gives the most accurate momentum thickness cannot be determined; however, in order to be consistent, the measured temperature-velocity relationship was also used to determine the momentum thickness. The measured-temperature-velocity relationship is shown in figure 10 in which the total-temperature ratio is plotted against the velocity ratio squared.

An expression for the ratio of the velocity in the boundary layer to the velocity at the edge of the boundary layer is as follows:

$$\frac{u}{U_\delta} = \frac{M}{M_\delta}\sqrt{\frac{1 + 0.2M_\delta^2}{1 + 0.2M^2}\,\frac{T_t}{T_{t,\delta}}} \tag{7}$$

The Mach number distribution was obtained from the ratio of the pitot-survey pressure to the static pressure. The static pressure was assumed to be constant through the boundary layer.

With the Mach number distribution and the Mach number at the edge of the boundary layer known, the other two unknowns of equation (7) (i.e., the ratios u/U_δ and $T_t/T_{t,\delta}$) were determined by an iterative process. First, a total-temperature ratio $T_t/T_{t,\delta}$ was chosen and then a velocity ratio u/U_δ was

calculated by using equation (7). This calculated u/U_δ was then used to find a new $T_t/T_{t,\delta}$ from figure 10. This process was repeated until agreement was reached between the two values of $T_t/T_{t,\delta}$. The boundary-layer pressure, Mach number, and velocity ratios for each of the seven survey stations are presented in table I.

With the total-temperature ratio $T_t/T_{t,\delta}$ and velocity ratio u/U_δ known, the boundary-layer momentum thickness for the cylinder was calculated by using the following equation:

$$\theta = \int_0^\delta \frac{\rho u}{\rho_\delta U_\delta}\left(1 - \frac{u}{U_\delta}\right)\frac{r + y}{r}\,dy \tag{8}$$

where $\frac{\rho}{\rho_\delta} = \frac{T_\delta}{T}$. The displacement thickness was calculated by using the following equation:

$$\delta^* = \int_0^\delta \left(1 - \frac{\rho u}{\rho_\delta U_\delta}\right)\frac{r + y}{r}\,dy \tag{9}$$

The boundary-layer thickness δ_{pr} was determined by plotting the boundary-layer survey pressures p' against the measured height y in the boundary layer. An example of one such plot is shown in figure 12. Points outside the boundary layer are at a nearly constant pressure. The intersection of a straight line drawn through these points and a straight line drawn through the last few data points just inside the edge of the boundary layer was taken to be the total thickness. The velocity ratio at the total thickness when found in this manner was approximately 0.998.

Values of boundary-layer momentum and displacement thicknesses and of boundary-layer thickness based on pitot-pressure profiles are presented in table III, along with the skin-friction coefficients and Reynolds numbers.

Turbulent Velocity Profiles

The nondimensional velocity profiles for the different stations are plotted in figure 13 as u/U_δ against y/θ. Power profiles, one-seventh and one-ninth, are also plotted to serve as a basis for comparison. The profiles indicate that n decreases somewhat with an increase in Reynolds number and becomes constant at the last three stations (fig. 13(b)) where the profiles correspond to a one-eighth power. The profile at the 8-inch station (fig. 13(a)) corresponds more closely to a one-ninth power which is a higher value of n for the measured value of R_θ than that indicated in a correlation of n with R_θ given in reference 15. It is unlikely that the larger value of n is associated with incomplete transition at the 8-inch station,

inasmuch as reference 16 indicates that natural transition should be completed at an approximate Reynolds number of 5×10^6 or, in this case, 6 inches.

In order to see whether the transition trip was causing any distortion in the profiles, a survey of the boundary layer was made at the 11-inch station with a smooth leading edge on the model. By a comparison in figure 13(c), the smooth-leading-edge profile is seen to correspond to some profile between the 8- and 11-inch stations. This result is to be expected since transition occurred later on the smooth model, as shown by the schlieren photographs (figs. 14(a) and (b)); therefore, the effective Reynolds number of this profile would be lower than that of the 11-inch station with a transition trip. Since the profiles with a transition trip have the same general shape as the profile with natural transition, it is believed that there was no distortion effect due to the transition trip.

It is of interest to note here that even though the profiles correspond to a changing power profile with Reynolds number, the shape factor δ^*/θ was found to be relatively constant except for the 5-inch station which is thought to be in the region of transitional flow. These shape factors for the different stations are presented in table III. An average value for δ^*/θ was found to be 16.9 with a variation of less than 2 percent. This nearly constant shape factor is to be expected since, for a power-law profile of the form $\frac{u}{U_\delta} = \left(\frac{y}{\delta}\right)^{1/n}$, it is relatively independent of the value of n. This relative independence is shown in figure 15 in which the shape factor δ^*/θ is plotted against n. Little variation of δ^*/θ with n is shown, especially at the higher values of n. The transverse curvature of the boundary layer is indicated by the factor δ/r. The effect of this factor on the shape factor δ^*/θ is also shown in figure 15. The effect of δ/r is seen to be negligible for the maximum δ/r encountered in this investigation, that is, $\delta/r \approx 1/5$.

Theoretical values of δ/θ are shown in figure 15. They are seen to vary considerably with both δ/r and n. The method from which the theoretical curves of figure 15 were calculated is presented in the appendix.

Skin Friction

One of the main objectives of this investigation was to determine average skin-friction coefficients for the turbulent boundary layer by the momentum method at a Mach number of 6 and adiabatic-wall conditions.

Longitudinal Mach number distribution.- The Mach number distribution along the top of the model obtained from probe total pressures, static pressures, and the tunnel stagnation pressure is shown in figure 16. The Mach number increases from about 5.95 at 5 inches to 6.02 at 40 inches. The skin-friction coefficients should be obtained when the flow conditions along the edge of the boundary layer are constant. In reference 6 Wilson compensated for a change in Mach number from the front of the model to the survey station by integrating his momentum thicknesses across a fictitious plane removed from the survey plane. The conditions outside the boundary layer of this fictitious plane correspond

to the average Mach number along the entire model, that is, $\bar{M}_\delta$. In the nomenclature of this report, Wilson's equation for the momentum thickness at the fictitious plane in terms of the conditions at the survey plane and the Mach number outside the boundary layer at the two planes is

$$\bar{\theta} = \frac{M_\delta}{\bar{M}_\delta}\left(\frac{1 + \frac{\gamma - 1}{2}\bar{M}_\delta^2}{1 + \frac{\gamma - 1}{2}M_\delta^2}\right)^{\frac{\gamma+1}{2(\gamma-1)}} \int_0^\delta \frac{\rho u}{\rho_\delta U_\delta}\left\{1 - \sqrt{1 - \left(\frac{M_\delta}{\bar{M}_\delta}\right)^2\left[1 - \left(\frac{u}{U_\delta}\right)^2\right]}\right\} dy \qquad (10)$$

Instead of tediously integrating $\bar{\theta}$ from the survey data, a procedure similar to that of Wilson's was followed; the ratio $\bar{\theta}/\theta$ for different values of M_δ was calculated by assuming the following velocity distribution:

$$\frac{u}{U_\delta} = \left(\frac{y}{\delta}\right)^{1/9} \qquad (11)$$

The momentum-thickness ratio is plotted against the ratio of the Mach numbers of the two planes $M_\delta/\bar{M}_\delta$ in figure 17. The algebraic average Mach number over the entire cylinder was calculated to be 5.98 $\left(\text{i.e., } \bar{M}_\delta = 5.98\right)$. Since the Mach number along the model did not vary greatly, this correction to θ was very small, being less than 1.5 percent.

Determination of virtual origin.- Since all theoretical analyses are based on the assumption of fully developed turbulent flow from the leading edge, the region of laminar flow in this test has to be taken into account and, as explained in reference 2, can be done by finding the fictitious (virtual) origin of the turbulent boundary layer. The Reynolds number based on the length from the virtual origin is the effective Reynolds number of the turbulent boundary layer.

The various methods for determining the position of this origin are described in reference 2. Two of these methods were applied to the present data. The first method used was the extrapolation of the momentum thickness, measured in the turbulent portions of the boundary layer, to zero. This extrapolation was done by assuming a growth of the boundary layer of the following form:

$$R_{\bar{\theta}} = K\left(R_{l_e} - R_{l_{e-x}}\right)^C \qquad (12)$$

This mathematical curve was fitted to the experimental data by the method of least squares. Values obtained for $R_{l_{e-x}}$ and C were 1.56×10^6 and 0.679, respectively, and when substituted into equation (12) yield a virtual origin that is about 1.87 inches downstream from the leading edge.

The second method used was that of Rubesin, Maydew, and Varga (ref. 17). In this method the same type of power equation is assumed for the growth of the boundary layer, but the constant C is obtained by averaging the values predicted by several theories. For the conditions of this investigation, the average value of C used was 0.800, the data were plotted on log-log paper, and the value of R_{le-x} necessary to match the slope of the line C = 0.800 was obtained. This procedure yielded a value of R_{le-x} of -0.04×10^6. Therefore, the virtual origin by this method is 0.05 inch upstream from the leading edge.

A plot of $R_{\bar{\theta}}$ against the Reynolds number based on the distance from the leading edge R_{le} is shown in figure 18(a). Station 1 (5-inch station) is thought to be in the region of transition (note data symbol labeled "transitional flow" in fig. 18(a)). Besides the fact that this data symbol does not fall in line with the data from the other stations, the schlieren photo of figure 14(b) indicates that this station is in the transitional flow region. Consequently, the momentum thickness from this station was not used in the determination of the virtual origin of the turbulent boundary layer.

Figure 18(b) shows a plot of $R_{\bar{\theta}}$ against the Reynolds number based on the distance from the virtual origin as found by the two methods. Since it is not known which of the two methods is more accurate, it is considered that the actual virtual origin could be at any point between the calculated virtual origins.

Average skin-friction coefficients.- The average skin-friction coefficients can be determined from the equation

$$C_F = 2 \frac{R_{\bar{\theta}}}{R_x} \tag{13}$$

if the virtual origin is known so that the effective Reynolds number R_x can be determined. A plot of the average skin-friction coefficients at various Reynolds numbers, determined by using the calculated virtual origins, is shown in figure 19. Also shown in the figure are four turbulent skin-friction theories. The variation of the average skin-friction coefficients due to the difference in the virtual origins is seen to be rather large at the front stations (20-percent variation from the average at the most forward station presented). This variation decreases with increasing Reynolds number and at the back stations is only about 3 percent.

Since the present experimental values of C_F are for a cylinder, the theoretical values of C_F for a flat plate should be modified to take into account the effect of the lateral surface curvature. An increase in C_F of about 1 percent because of surface curvature is shown in reference 18 for a ratio of boundary-layer thickness to cylinder radius of 0.18. This ratio of 0.18 is the largest ratio of boundary-layer thickness to cylinder radius

occurring in this investigation. The correction at any forward station would be less. For the incompressible case, references 19 and 20 also give a correction of about 1 percent at the last station. Since the effect of curvature is seen to be so small, no attempt was made to correct the skin-friction coefficients.

The average skin-friction data are replotted in figure 20 as ratios to the incompressible skin-friction coefficients. The incompressible skin-friction coefficient was obtained from the well-known Kármán-Schoenherr equation for average skin-friction coefficient in incompressible flow. From figures 19 and 20 it can be seen that it would be difficult to say that the experimental average skin-friction coefficients correspond to any one particular theory because of the uncertainty at low Reynolds numbers. At the high Reynolds numbers where the exact location of the virtual origin is not as important, the coefficients are between the values predicted by the theory of Wilson and Van Driest and the T' method of Sommer and Short.

Along with the present data, other authors' experimental values of average skin-friction coefficients (refs. 1, 6, 17, 21, and 22) are presented in figure 21. Here the ratio of the skin-friction coefficient to the Kármán-Schoenherr incompressible coefficient is plotted against Mach number at a constant Reynolds number of 10×10^6. Since the choice of a Reynolds number of 10×10^6 for figure 21 was an arbitrary one, it should be noted that the relation between the present data and the theories would change for any other Reynolds number chosen. This changing relation can be seen by referring to figure 20.

As figure 21 shows, the average skin-friction data available at this time were obtained at Mach numbers less than 4 and, therefore, comparison with the present data is difficult. Local skin-friction data, however, have been obtained at higher Mach numbers by Korkegi (ref. 23) and Matting, Chapman, Nyholm, and Thomas (ref. 24). Therefore, local skin-friction coefficients were obtained from the present data for comparison.

Local skin-friction coefficients.- The local skin-friction coefficient for the present data was obtained from the rate of growth of the measured momentum thickness by differentiating the following equation of the curves in figure 18(b) which are of the form

$$R_{\bar{\theta}} = KR_x^C \tag{14}$$

and then using the equation

$$C_f = 2 \frac{dR_{\bar{\theta}}}{dR_x} \tag{15}$$

In figure 22, local skin-friction data are plotted against Mach number in a manner similar to that of figure 21 for the average skin-friction data.

Experimental local skin-friction coefficients obtained by other authors were also plotted in figure 22 and these data can be found in references 17 and 23 to 26. Korkegi obtained local skin-friction coefficients from force-balance measurements at a Mach number of 5.8 and Reynolds numbers from 2.3×10^6 to 3.9×10^6. The data were extrapolated, as is to be explained, to $R_x = 10 \times 10^6$ for figure 22 of this report. Matting and coauthors (ref. 24) also used the skin-friction balance to obtain local coefficients at Mach numbers of 2.95 and 4.2 in air. Then, in helium flow, local skin-friction data were obtained at equivalent air Mach numbers of 4.2, 6.7, and 9.9. The Reynolds number variation was from 2×10^6 to 100×10^6. It was found that the data from the measurements in air and helium agreed very well at the Mach number of 4.2, but no comparison is available at the higher Mach numbers.

Figure 22 shows how the present data compare with these two sets of data. Korkegi's coefficient at a Mach number of 5.8 is about 12 percent higher than the present data, whereas the level of Matting's high Mach number data obtained in helium is considerably lower than that of the present data. The plotted point for Korkegi's data was obtained by extrapolating the experimental values of C_f and the effective Reynolds numbers $\left(R_{x,max} \approx 5.5 \times 10^6\right)$, as determined in reference 2, to the Reynolds number of 10×10^6. (Other extrapolated points in figs. 21 and 22 were obtained in a similar manner.) Korkegi's data are such that considerable variation of the extrapolation is possible, and the bar through the plotted point gives an indication of this variation.

In reference 2, a comparison of data available at that time indicates that the Sommer and Short T' method appeared to provide the most accurate estimate of skin friction within the ranges of Mach number, Reynolds number, and heat transfer of the available experiments. The present data, however, casts doubt as to which theory will provide reliable estimates of skin friction at Mach numbers greater than 4. Additional experimental research on turbulent skin friction is required at hypersonic speeds.

CONCLUSIONS

An investigation of the turbulent boundary layer on a hollow cylinder at a Mach number of 6, at Reynolds numbers up to 33×10^6, and for adiabatic-wall conditions leads to the following conclusions:

1. For the turbulent boundary layer at a Mach number of 6, the temperature recovery factor was found to be approximately 0.88. This value is in very good agreement with values of other experiments. A gradual decrease in recovery factor with an increase in Reynolds number was obtained which is also in accord with findings of other investigations.

2. The experimentally determined total-temperature-velocity relationship did not agree with any of the three theoretical distributions considered: the assumption of a constant total temperature, the quadratic distribution used by Donaldson in NACA RM L52H04, and the Crocco laminar distribution used by

Van Driest in NACA TN 2597. However, the momentum thickness calculated by assuming a constant total temperature agreed well with the momentum thickness determined with the experimentally measured temperature distribution. The absence of a good theory for the temperature-velocity relationship in turbulent boundary layers is a problem which merits more attention.

3. A comparison of measured velocity profiles with a power-law velocity profile of the form $\frac{u}{U_\delta} = \left(\frac{y}{\delta}\right)^{1/n}$ (where δ is the boundary-layer thickness) showed a decrease in the exponent n from 9 at a Reynolds number of about 6×10^6 (8-inch station) to 8 at a Reynolds number of approximately 32×10^6 (40-inch station). The value of n at the lower Reynolds number was somewhat greater than that indicated by the correlation of experimental data in NAVORD Rept. 3854 by Persh. The boundary-layer shape factor, however, was found to be relatively constant at a value of approximately 16.9, which agrees well with the theoretical shape factor for a power-velocity profile.

4. There was considerable uncertainty in the average skin-friction coefficient at low Reynolds numbers as a result of the difference in the position of the virtual origin as calculated by the methods of least squares and of Rubesin, Maydew, and Varga (NACA TN 2305). This uncertainty made it difficult to compare the data with theories in the low Reynolds number range. At the higher Reynolds numbers, however, the uncertainty in the value of the skin-friction coefficient was less and the coefficients were between the values predicted by the theory of Wilson and Van Driest and the T' method of Sommer and Short. Exact establishment of the hypersonic turbulent skin-friction level requires additional experimental research.

Langley Research Center,
National Aeronautics and Space Administration,
Langley Station, Hampton, Va., March 19, 1965.

APPENDIX

EQUATIONS FOR DETERMINATION OF δ^*/θ AND δ/θ FOR POWER-LAW BOUNDARY-LAYER VELOCITY PROFILES ON A CYLINDER

The nondimensional equations for δ^* and θ for the turbulent boundary layer on a cylinder are as follows:

$$\frac{\delta^*}{\delta} = \int_0^1 \left(1 - \frac{\rho u}{\rho_\delta U_\delta}\right)\left(1 + \frac{\delta}{r}\frac{y}{\delta}\right) d\,\frac{y}{\delta} \tag{A1}$$

$$\frac{\theta}{\delta} = \int_0^1 \frac{\rho u}{\rho_\delta U_\delta}\left(1 - \frac{u}{U_\delta}\right)\left(1 + \frac{\delta}{r}\frac{y}{\delta}\right) d\,\frac{y}{\delta} \tag{A2}$$

If the assumptions of a constant total temperature and pressure through the boundary layer and a power-profile variation of velocity through the boundary layer of the form $\frac{u}{U_\delta} = \left(\frac{y}{\delta}\right)^{1/n}$ are made, then exact solutions for equations (A1) and (A2) can be obtained in the following way. For a constant total temperature through the boundary layer, the following energy equation is true for all points in the boundary layer:

$$\frac{u^2}{2} + c_p T = c_p T_t = c_p T_{t,\delta}$$

The density distribution is

$$\frac{\rho_\delta}{\rho} = \frac{T_{t,\delta}}{T_\delta} - \left(\frac{T_{t,\delta}}{T_\delta} - 1\right)\left(\frac{u}{U_\delta}\right)^2$$

By setting $z = \frac{u}{U_\delta} = \left(\frac{y}{\delta}\right)^{1/n}$, $a = \frac{T_\delta}{T_{t,\delta}}$, and $b = 1 - \frac{T_\delta}{T_{t,\delta}}$, equation (A1) becomes

$$\frac{\delta^*}{\delta} = \int_0^1 \left(1 - \frac{az}{1 - bz^2}\right)\left(1 + \frac{\delta}{r} z^n\right) n z^{n-1}\, dz$$

When the integral is split and simplified, this equation becomes

$$\frac{\delta^*}{\delta} = 1 - na \int_0^1 \frac{z^n}{1 - bz^2}\,dz + \frac{1}{2}\frac{\delta}{r} - \frac{\delta}{r}\,na \int_0^1 \frac{z^{2n}}{1 - bz^2}\,dz \tag{A3}$$

The first two terms are those obtained for a flat plate in reference 27.

If n takes on integer values, the exact solutions to the integral equation (A3) for δ^*/δ can be written in series form. The series solution for values of n which are odd integers can be written in the following summation form:

$$\frac{\delta^*}{\delta} = 1 + \frac{1}{2}\frac{\delta}{r} + \frac{n}{2}\frac{a}{b^{(n+1)/2}}\left(\sum_{i=1}^{\frac{n-1}{2}} \frac{b^i}{i} + \log_e a\right)$$

$$+ \frac{\delta}{r}\,n\,\frac{a}{b^n}\left(\sum_{i=0}^{n-1} \frac{b^i}{2i + 1} - \frac{1}{2\sqrt{b}} \log_e \frac{1 + \sqrt{b}}{1 - \sqrt{b}}\right) \tag{A4}$$

In finding a similar equation for the momentum thickness, the quantities a, b, and z are substituted into equation (A2) and the following equation is obtained:

$$\frac{\theta}{\delta} = na \int_0^1 \left(\frac{1 - z}{1 - bz^2}\right) z^n \left(1 + \frac{\delta}{r}\,z^n\right) dz \tag{A5}$$

When the values of n are restricted to odd integers, the results of the integrals in equation (A5) can be written in summation form as follows:

$$\frac{\theta}{\delta} = \frac{n}{2}\frac{a}{b^{(n+1)/2}}\left[2 - \log_e a + \frac{1}{\sqrt{b}} \log_e \frac{1 - \sqrt{b}}{1 + \sqrt{b}} - \sum_{i=1}^{\frac{n-1}{2}} \frac{b^i}{i(2i + 1)}\right]$$

$$+ \frac{\delta}{r}\,\frac{n}{2}\,\frac{a}{b^n}\left[\frac{1}{b} \log_e a - \frac{1}{\sqrt{b}} \log_e \frac{1 - \sqrt{b}}{1 + \sqrt{b}} - \sum_{i=0}^{n-1} \frac{b^i}{(i + 1)(2i + 1)}\right] \tag{A6}$$

Equations (A4) and (A6) were used to obtain the values of δ^*/θ and δ/θ in figure 15.

REFERENCES

1. Chapman, Dean R.; and Kester, Robert H.: Turbulent Boundary-Layer and Skin-Friction Measurements in Axial Flow Along Cylinders at Mach Numbers Between 0.5 and 3.6. NACA TN 3097, 1954.

2. Peterson, John B., Jr.: A Comparison of Experimental and Theoretical Results for the Compressible Turbulent-Boundary-Layer Skin Friction With Zero Pressure Gradient. NASA TN D-1795, 1963.

3. Sommer, Simon C.; and Short, Barbara J.: Free-Flight Measurements of Turbulent-Boundary-Layer Skin Friction in the Presence of Severe Aerodynamic Heating at Mach Numbers From 2.8 to 7.0. NACA TN 3391, 1955.

4. Van Driest, E. R.: Turbulent Boundary Layer in Compressible Fluids. J. Aeron. Sci., vol. 18, no. 3, Mar. 1951, pp. 145-160, 216.

5. Wilson, Robert E.: Turbulent Boundary-Layer Characteristics at Supersonic Speeds - Theory and Experiment. J. Aeron. Sci., vol. 17, no. 9, Sept. 1950, pp. 585-594.

6. Wilson, R. E.: Characteristics of Turbulent Boundary Layer Flow Over a Smooth, Thermally Insulated Flat Plate at Supersonic Speeds. DRL-301, CM-712 (Contract NOrd-9195), Univ. of Texas, June 1, 1952.

7. Van Driest, E. R.: The Turbulent Boundary Layer With Variable Prandtl Number. Rept. No. AL-1914, North Am. Aviation, Inc., Apr. 2, 1954.

8. Cope, W. F.: The Turbulent Boundary Layer in Compressible Flow. R. & M. No. 2840, Brit. A.R.C., 1953.

9. Monaghan, R. J.; and Johnson, J. E.: The Measurement of Heat Transfer and Skin Friction at Supersonic Speeds. Part II - Boundary Layer Measurements on a Flat Plate at $M = 2.5$ and Zero Heat Transfer. C.P. No. 64, Brit. A.R.C., Dec. 1952.

10. Sterrett, James R.; and Emery, James C.: Extension of Boundary-Layer-Separation Criteria to a Mach Number of 6.5 by Utilizing Flat Plates With Forward-Facing Steps. NASA TN D-618, 1960.

11. Stalder, Jackson R.; Rubesin, Morris W.; and Tendeland, Thorval: A Determination of the Laminar-, Transitional-, and Turbulent-Boundary-Layer Temperature-Recovery Factors on a Flat Plate in Supersonic Flow. NACA TN 2077, 1950.

12. Brevoort, Maurice J.; and Arabian, Barbara D.: Summary of Experimental Heat-Transfer Measurements in Turbulent Flow for a Mach Number Range From 0.87 to 5.05. NACA TN 4248, 1958.

13. Donaldson, Coleman duP.: Heat Transfer and Skin Friction for Turbulent Boundary Layers on Heated or Cooled Surfaces at High Speeds. NACA RM L52H04, 1952.

14. Van Driest, E. R.: Investigation of Laminar Boundary Layer in Compressible Fluids Using the Crocco Method. NACA TN 2597, 1952.

15. Persh, Jerome: A Theoretical Investigation of Turbulent Boundary Layer Flow With Heat Transfer at Supersonic and Hypersonic Speeds. NAVORD Rept. 3854, U.S. Naval Ord. Lab. (White Oak, Md.), May 19, 1955.

16. Holloway, Paul F.; and Sterrett, James R.: Effect of Controlled Surface Roughness on Boundary-Layer Transition and Heat Transfer at Mach Numbers of 4.8 and 6.0. NASA TN D-2054, 1964.

17. Rubesin, Morris, W.; Maydew, Randall C.; and Varga, Steven A.: An Analytical and Experimental Investigation of the Skin Friction of the Turbulent Boundary Layer on a Flat Plate at Supersonic Speeds. NACA TN 2305, 1951.

18. Eckert, Hans U.: Simplified Treatment of the Turbulent Boundary Layer Along a Cylinder in Compressible Flow. J. Aeron. Sci., vol. 19, no. 1, 1952, pp. 23-28, 38.

19. Landweber, L.: Effect of Transverse Curvature on Frictional Resistance. Rept. 689, David W. Taylor Model Basin, Navy Dept., March 1949.

20. Ginevskii, A. S.; and Solodkin, E. E.: The Effect of Lateral Surface Curvature on the Characteristics of Axially-Symmetric Turbulent Boundary Layers. J. Appl. Math. Mech., vol. 22, no. 6, 1958, pp. 1169-1179.

21. O'Donnell, Robert M.: Experimental Investigation at a Mach Number of 2.41 of Average Skin-Friction Coefficients and Velocity Profiles for Laminar and Turbulent Boundary Layers and an Assessment of Probe Effects. NACA TN 3122, 1954.

22. Brinich, Paul F.; and Diaconis, Nick S.: Boundary-Layer Development and Skin Friction at Mach Number 3.05. NACA TN 2742, 1952.

23. Korkegi, Robert H.: Transition Studies and Skin-Friction Measurements on an Insulated Flat Plate at a Mach Number of 5.8. J. Aeron. Sci., vol. 23, no. 2, Feb. 1956, pp. 97-107, 192.

24. Matting, Fred W.; Chapman, Dean R.; Nyholm, Jack R.; and Thomas, Andrew G.: Turbulent Skin Friction at High Mach Numbers and Reynolds Numbers in Air and Helium. NASA TR R-82, 1961.

25. Coles, Donald: Measurements in the Boundary Layer on a Smooth Flat Plate in Supersonic Flow. III. Measurements in a Flat-Plate Boundary Layer at the Jet Propulsion Laboratory. Rept. No. 20-71 (Contract No. DA-04-495-Ord 18), Jet Propulsion Lab., C.I.T., June 1, 1953.

26. Shutts, W. H.; Hartwig, W. H.; and Weiler, J. E.: Final Report on Turbulent Boundary-Layer and Skin-Friction Measurements on a Smooth, Thermally Insulated Flat Plate at Supersonic Speeds. DRL-364, CM-823 (Contract NOrd-9195), Univ. of Texas, Jan. 5, 1955.

27. Bradfield, W. S.: Research on Laminar and Turbulent Boundary Layers at Supersonic Speeds - Final Summary Report. Res. Rept. No. 131 (AFOSR TR-57-64, AD No. 136 559), Inst. Technol., Dept. Aeron. Eng., Univ. of Minnesota, Dec. 1957.

TABLE I.- BOUNDARY-LAYER PRESSURE, MACH NUMBER, AND VELOCITY DISTRIBUTIONS

(a) Station 1: x_{le} = 5.0 in.; T_δ = 109° R; T_t = 878° R; M_δ = 5.95; p_δ = 0.353 psia; and p_t = 523 psia

y, in.	$\frac{p_\delta}{p'}$	$\frac{M}{M_\delta}$	$\frac{u}{U_\delta}$
0.0035	0.2788	0.259	0.5855
.0035	.2102	.305	.6525
.0079	.1618	.353	.713
.0094	.1192	.416	.778
.0121	.0951	.469	.824
.0162	.0804	.512	.855
.0218	.0641	.576	.894
.0288	.0571	.611	.9115
.0372	.0522	.640	.9345
.0520	.0415	.720	.9535
.0668	.0335	.803	.974
.0793	.0294	.859	.984
.0964	.0245	.941	.994
.1172	.0219	.996	.9995
.1387	.0212	1.013	1.001
.1637	.0210	1.017	1.0015
.1998	.0209	1.019	1.002

TABLE I.- BOUNDARY-LAYER PRESSURE, MACH NUMBER, AND VELOCITY DISTRIBUTIONS - Continued

(b) Station 2: x_{le} = 6.0 in.; T_δ = 108° R; T_t = 872° R; M_δ = 5.95; p_δ = 0.349 psia; and p_t = 523 psia

y, in.	$\frac{p_\delta}{p'}$	$\frac{M}{M_\delta}$	$\frac{u}{U_\delta}$
0.0035	0.2404	0.282	0.620
.0045	.2354	.286	.627
.0086	.2079	.307	.655
.0154	.1328	.393	.756
.0237	.0929	.474	.8275
.0365	.0642	.575	.893
.0490	.0556	.619	.9155
.0617	.0476	.671	.9365
.0870	.0353	.782	.970
.1122	.0283	.874	.986
.1375	.0235	.959	.996
.1501	.0226	.980	.998
.1711	.0219	.996	.999
.2027	.0217	1.000	1.000

TABLE I.- BOUNDARY-LAYER PRESSURE, MACH NUMBER, AND VELOCITY DISTRIBUTIONS - Continued

(c) Station 3: x_{le} = 8.0 in.; T_δ = 108° R; T_t = 871° R; M_δ = 5.95; p_δ = 0.344 psia; and p_t = 519 psia

y, in.	$\frac{p_\delta}{p'}$	$\frac{M}{M_\delta}$	$\frac{u}{U_\delta}$
0.0035	0.2488	0.277	0.613
.0056	.2303	.289	.630
.0097	.2046	.310	.6595
.0104	.1805	.332	.688
.0181	.1227	.409	.7715
.0284	.0900	.482	.834
.0435	.0723	.540	.8735
.0604	.0600	.595	.9035
.0832	.0450	.690	.9435
.1108	.0342	.793	.9720
.1466	.0258	.915	.9915
.1785	.0226	.979	.9980
.2122	.0218	.998	1.0000
.2478	.0216	1.000	↓
.2880	.0216	1.000	
.3278	.0215	1.003	
.5452	.0214	1.007	1.0005

TABLE I.- BOUNDARY-LAYER PRESSURE, MACH NUMBER, AND VELOCITY DISTRIBUTIONS - Continued

(d) Station 4, natural transition: x_{le} = 11.0 in.; T_δ = 109° R; T_t = 883° R; M_δ = 5.96; p_δ = 0.347 psia; and p_t = 524 psia

y, in.	$\frac{p_\delta}{p'}$	$\frac{M}{M_\delta}$	$\frac{u}{U_\delta}$
0.0035	0.2358	0.286	0.6265
.0047	.2301	.290	.631
.0171	.1387	.383	.7455
.0314	.0956	.467	.822
.0429	.0835	.501	.848
.0636	.0690	.554	.881
.0803	.0571	.610	.911
.0975	.0479	.668	.9355
.1262	.0376	.756	.9635
.1565	.0295	.855	.9835
.2044	.0234	.962	.9965
.2829	.0214	1.005	1.0000
.3418	.0215	1.002	1.0000

TABLE I.- BOUNDARY-LAYER PRESSURE, MACH NUMBER, AND VELOCITY DISTRIBUTIONS - Continued

(e) Station 4: x_{le} = 11.0 in.; T_δ = 108° R; T_t = 872° R; M_δ = 5.96; p_δ = 0.345 psia; and p_t = 523 psia

y, in.	$\frac{p_\delta}{p'}$	$\frac{M}{M_\delta}$	$\frac{u}{U_\delta}$
0.0035	0.2534	0.273	0.607
.0035	.2480	.277	.613
.0068	.2349	.286	.626
.0112	.2051	.309	.658
.0155	.1501	.367	.7285
.0236	.1221	.410	.772
.0405	.0935	.472	.826
.0507	.0849	.496	.8445
.0616	.0761	.525	.864
.0869	.0598	.595	.9035
.1123	.0473	.671	.9365
.1373	.0381	.750	.962
.1645	.0311	.831	.980
.1906	.0267	.899	.9895
.2198	.0239	.951	.9955
.2385	.0227	.976	.998
.2697	.0219	.993	.999
.2933	.0219	.994	.9995

TABLE I.- BOUNDARY-LAYER PRESSURE, MACH NUMBER, AND VELOCITY DISTRIBUTIONS - Continued

(f) Station 5: x_{le} = 33.0 in.; T_δ = 106° R; T_t = 871° R; M_δ = 6.02; p_δ = 0.325 psia; and p_t = 523 psia

y, in.	$\frac{p_\delta}{p'}$	$\frac{M}{M_\delta}$	$\frac{u}{U_\delta}$
0.0035	0.2484	0.274	0.608
.0035	.2478	.274	.608
.0065	.2405	.279	.6155
.0085	.2314	.285	.625
.0166	.1845	.324	.6775
.0249	.1568	.354	.714
.0331	.1442	.371	.733
.0444	.1337	.386	.749
.0570	.1261	.399	.761
.0697	.1194	.411	.774
.0950	.1049	.440	.800
.1202	.0936	.467	.822
.1473	.0828	.498	.846
.1853	.0701	.543	.875
.2255	.0590	.593	.9025
.2803	.0468	.669	.9355
.3309	.0381	.743	.960
.3815	.0312	.822	.978
.4375	.0258	.905	.990
.4824	.0229	.961	.9965
.5331	.0217	.988	.999
.5964	.0214	.995	.9995
.6615	.0213	.997	1.0000

TABLE I.- BOUNDARY-LAYER PRESSURE, MACH NUMBER, AND VELOCITY DISTRIBUTIONS - Continued

(g) Station 6: x_{le} = 37.0 in.; T_δ = 105° R; T_t = 867° R; M_δ = 6.02; p_δ = 0.324 psia; and p_t = 523 psia

y, in.	$\frac{p_\delta}{p'}$	$\frac{M}{M_\delta}$	$\frac{u}{U_\delta}$
0.0035	0.2711	0.260	0.586
.0035	.2731	.259	.586
.0053	.2637	.264	.593
.0094	.2434	.277	.613
.0166	.1946	.315	.666
.0223	.1620	.348	.707
.0293	.1481	.366	.728
.0434	.1340	.386	.749
.0579	.1247	.401	.764
.0715	.1169	.415	.777
.0968	.1037	.442	.8005
.1222	.0920	.471	.826
.1474	.0821	.500	.847
.2009	.0646	.566	.888
.2499	.0528	.628	.9195
.3013	.0430	.697	.946
.3626	.0342	.784	.970
.4277	.0276	.874	.986
.4931	.0232	.955	.996
.5522	.0215	.993	.999
.6178	.0212	1.000	1.000
.6813	.0212	.999	1.000

TABLE I.- BOUNDARY-LAYER PRESSURE, MACH NUMBER, AND VELOCITY DISTRIBUTIONS - Continued

(h) Station 7: x_{le} = 40.0 in.; T_δ = 106° R; T_t = 871° R; M_δ = 6.02; p_δ = 0.326 psia; and p_t = 524 psia

y, in.	$\frac{p_\delta}{p'}$	$\frac{M}{M_\delta}$	$\frac{u}{U_\delta}$
0.0035	0.2464	0.276	0.612
.0037	.2454	.276	.612
.0066	.2368	.282	.620
.0097	.2229	.292	.6345
.0163	.1830	.326	.680
.0221	.1609	.350	.709
.0288	.1467	.368	.730
.0432	.1334	.387	.750
.0563	.1255	.401	.7635
.0684	.1188	.412	.774
.0948	.1058	.438	.7975
.1188	.0950	.464	.820
.1438	.0863	.488	.839
.1844	.0734	.531	.868
.2230	.0627	.576	.894
.2707	.0523	.633	.9215
.3230	.0434	.696	.946
.3864	.0346	.780	.9695
.4497	.0281	.867	.985
.5131	.0236	.949	.995
.5762	.0216	.991	.999
.6015	.0213	.998	1.000

TABLE I.- BOUNDARY-LAYER PRESSURE, MACH NUMBER, AND VELOCITY DISTRIBUTIONS - Concluded

(i) Station 7: x_{le} = 40.0 in.; T_δ = 104° R; T_t = 861° R; M_δ = 6.02; p_δ = 0.325 psia; and p_t = 523 psia

y, in.	$\frac{p_\delta}{p'}$	$\frac{M}{M_\delta}$	$\frac{u}{U_\delta}$
0.0053	0.2469	0.275	0.610
.0054	.2475	.275	.610
.0053	.2473	.275	.610
.0085	.2330	.284	.623
.0107	.2132	.299	.644
.0178	.1757	.333	.6895
.0222	.1591	.352	.711
.0304	.1432	.373	.735
.0446	.1300	.393	.756
.0599	.1208	.408	.7705
.0870	.1071	.435	.795
.1102	.0973	.458	.8145
.1496	.0828	.498	.846
.1880	.0706	.541	.874
.2492	.0555	.613	.9125
.3159	.0434	.695	.945
.3923	.0331	.798	.973
.4553	.0270	.886	.988
.5168	.0228	.963	.9965
.5832	.0211	1.002	1.0000
.6329	.0210	1.006	1.0000
.6979	.0210	1.004	1.0000

TABLE II.- TEMPERATURE SURVEY

[Station 5 (test 20): x_{le} = 33.0 in.; M_δ = 6.02; and p_t = 523.6 psia]

y, in.	$T_{t,\delta}$ (a)	T_p	T_t
0.0100	860	773	801
.0100	860	775	803
.0143	857	775	804
.0159	856	776	806
.0184	857	778	807
.0224	861	782	812
.0310	866	784	815
.0372	855	778	809
.0435	860	782	814
.0561	860	785	816
.0687	851	781	813
.1235	855	796	830
.1445	867	815	852
.1961	865	819	856
.2496	858	822	860
.2983	859	829	867
.3466	860	837	872
.4140	864	846	872
.4753	859	844	862
.5403	859	847	859

[a]Measured in settling chamber; assumed to be $T_{t,\delta}$.

TABLE III.- REDUCED DATA FROM PRESSURE-SURVEY MEASUREMENTS

Station	Test	x_{le}, in.	x, in.		M_δ	n	δ^*, in.	δ_{pr}, in.	θ, in.	$\frac{\delta^*}{\theta}$	$\bar{M}_\delta$	$\bar{\theta}$, in.	$R_{\bar{\theta}}$	R_x		C_F	
			(a)	(b)										(a)	(b)	(a)	(b)
c_1	63	5.0	3.13	5.05	5.95	13	0.0478	0.12	2.63×10^{-3}	18.2	5.98	2.67×10^{-3}	2.21×10^3	2.59×10^6	4.18×10^6	1.71×10^{-3}	1.06×10^{-3}
2	13	6.0	4.13	6.05	5.95	10	.0662	.15	3.93	16.9		3.98	3.29	3.41	5.01	1.93	1.31
3	15	8.0	6.13	8.05	5.95	9	.0820	.18	4.89	16.8		4.94	4.06	5.00	6.60	1.62	1.23
d_4	10	11.0	-----	-----	5.96	9	.101	.22	6.04	16.7		----------	----------	----------	----------	----------	----------
4	14	11.0	9.13	11.05	5.96	9	.115	.24	6.76	17.0		6.81	5.65	7.56	9.16	1.50	1.23
5	16	33.0	31.13	33.05	6.02	8	.281	.51	16.4	17.1		16.2	13.31	25.44	27.04	1.04	.981
6	26	37.0	35.13	37.05	6.02	8	.285	.53	16.8	17.0		16.5	13.7	29.14	30.74	.940	.891
7	17	40.0	38.13	40.05	6.02	8	.304	.56	18.0	16.9		17.7	14.6	31.14	32.74	.934	.889
7	18	40.0	38.13	40.05	6.02	8	.297	56	17.6	16.9	↓	17.4	14.2	31.24	32.84	.910	.866

[a]Virtual origin by least squares method.
[b]Virtual origin by method described by Rubesin, Maydew, and Varga (ref. 17).
[c]Flow in region of transition.
[d]Natural transition.

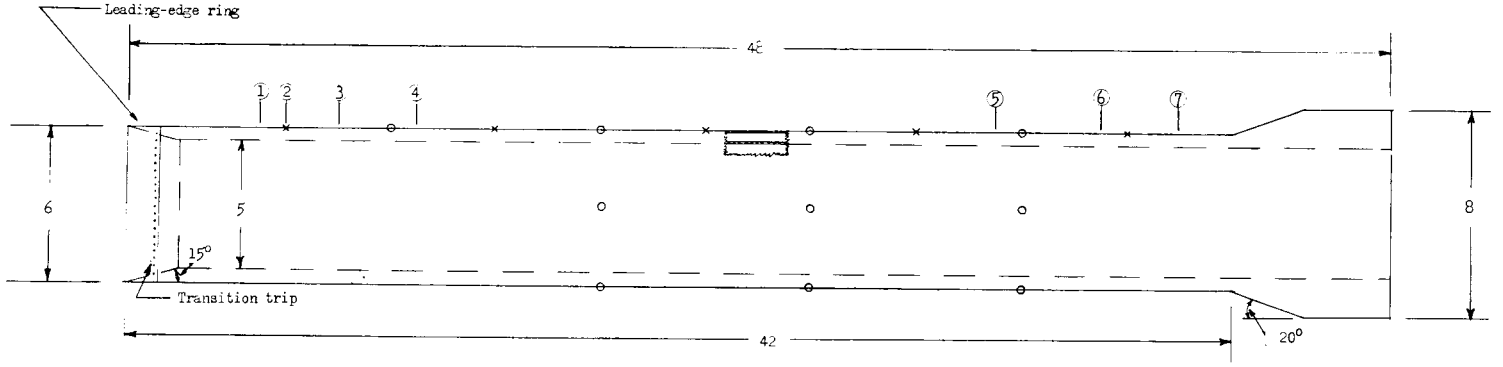

		x_{le}, inches
⚲	Stations	5, 6, 8, 11, 33, 37, 40
×	Thermocouples	6, 14, 22, 30, 38
○	Static orifices	10, 18, 26, 34

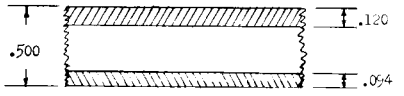

Enlarged cross section of wall

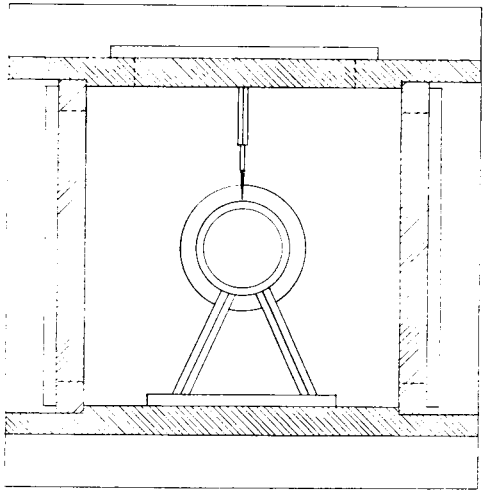

Front view

(mounted in tunnel)

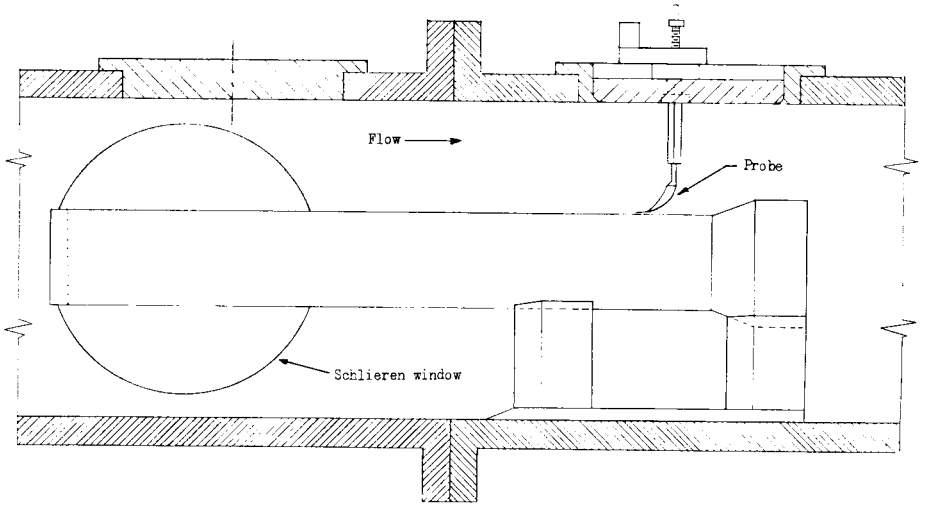

Side view

(mounted in tunnel)

Figure 1.- Hollow-cylinder model with dimensions and probe instrumentation. (All dimensions are in inches unless otherwise noted.)

L-63-9850

Figure 2.- Leading-edge ring showing transition trip with roughness height of 0.025 inch and diameter of 0.075 inch.

Front view

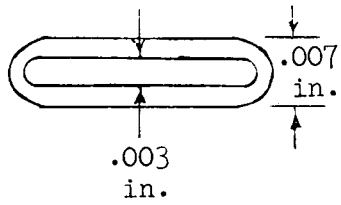

Enlarged view of probe tip

Side view

Figure 3.- Schematic of boundary-layer pressure probe.

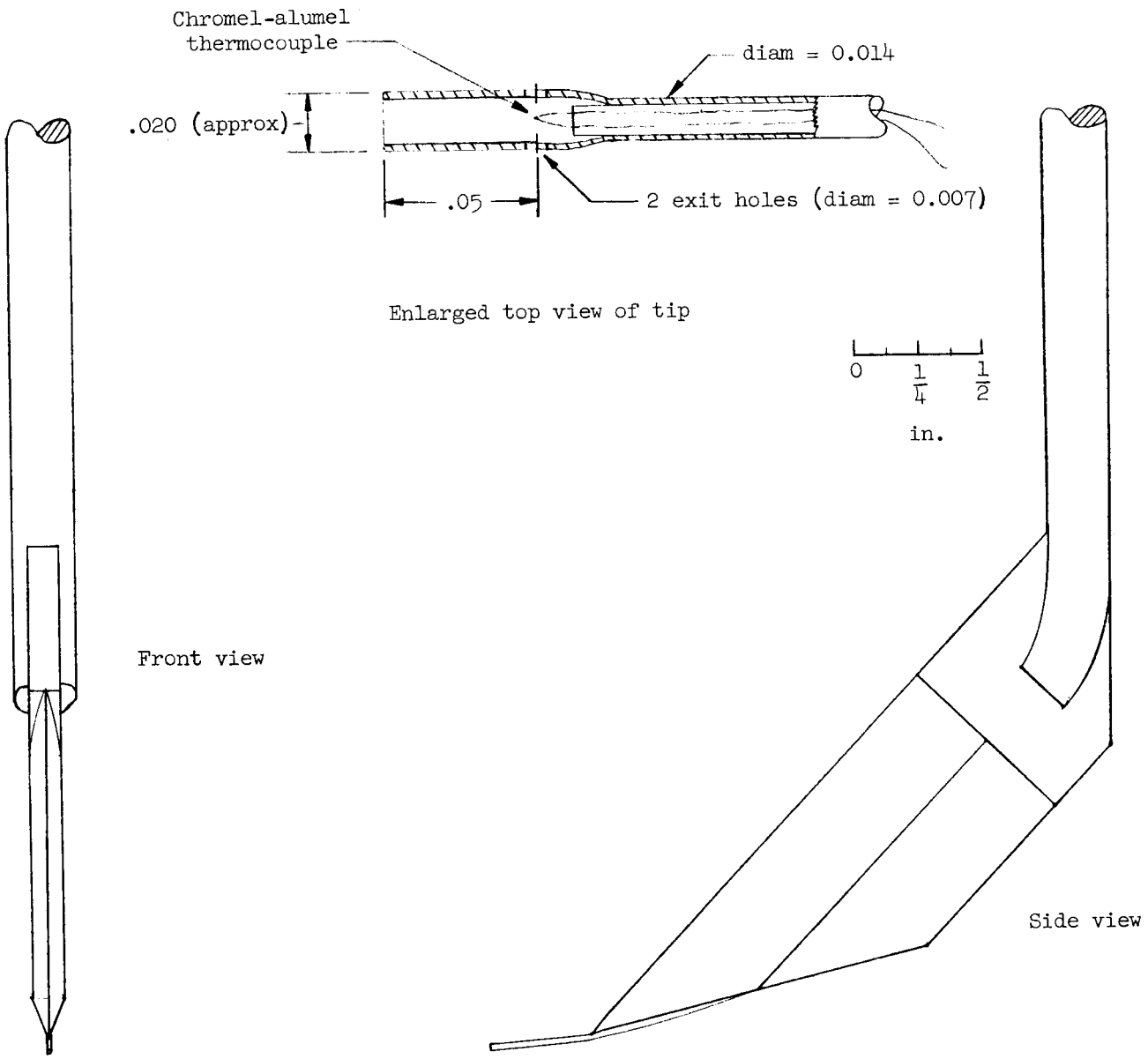

Figure 4.- Schematic of boundary-layer temperature probe. (All dimensions are in inches.)

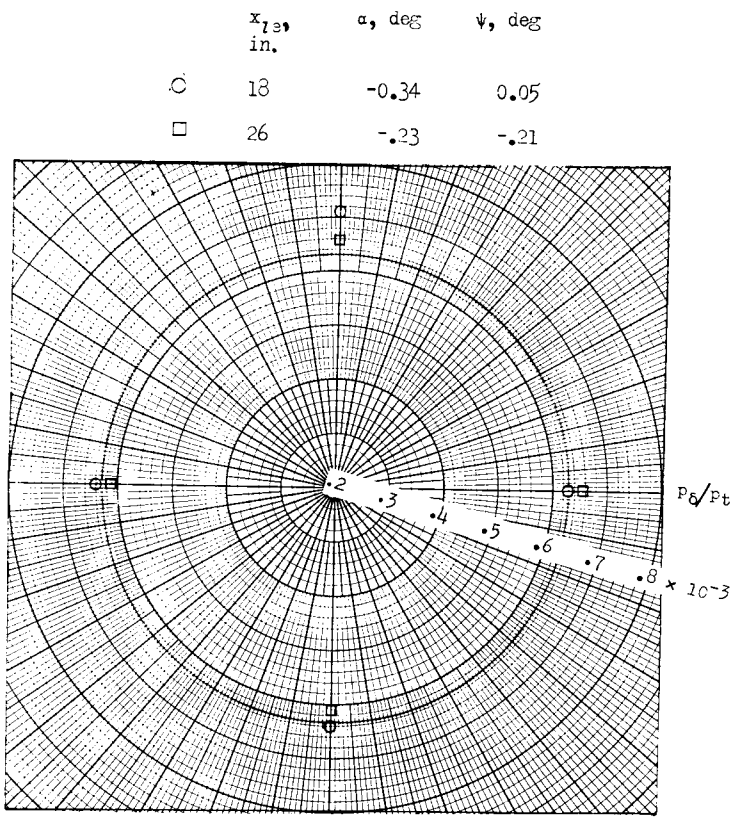

(a) Initial alinement.

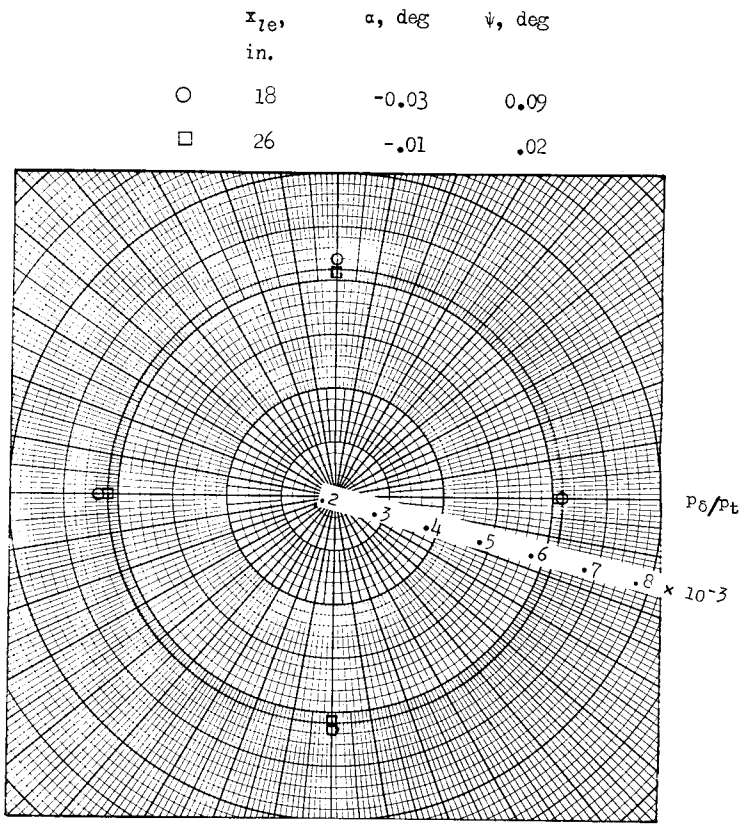

(b) Final alinement.

Figure 5.- Static-pressure distributions during alinement of model and calculated angles of attack and yaw (looking forward).

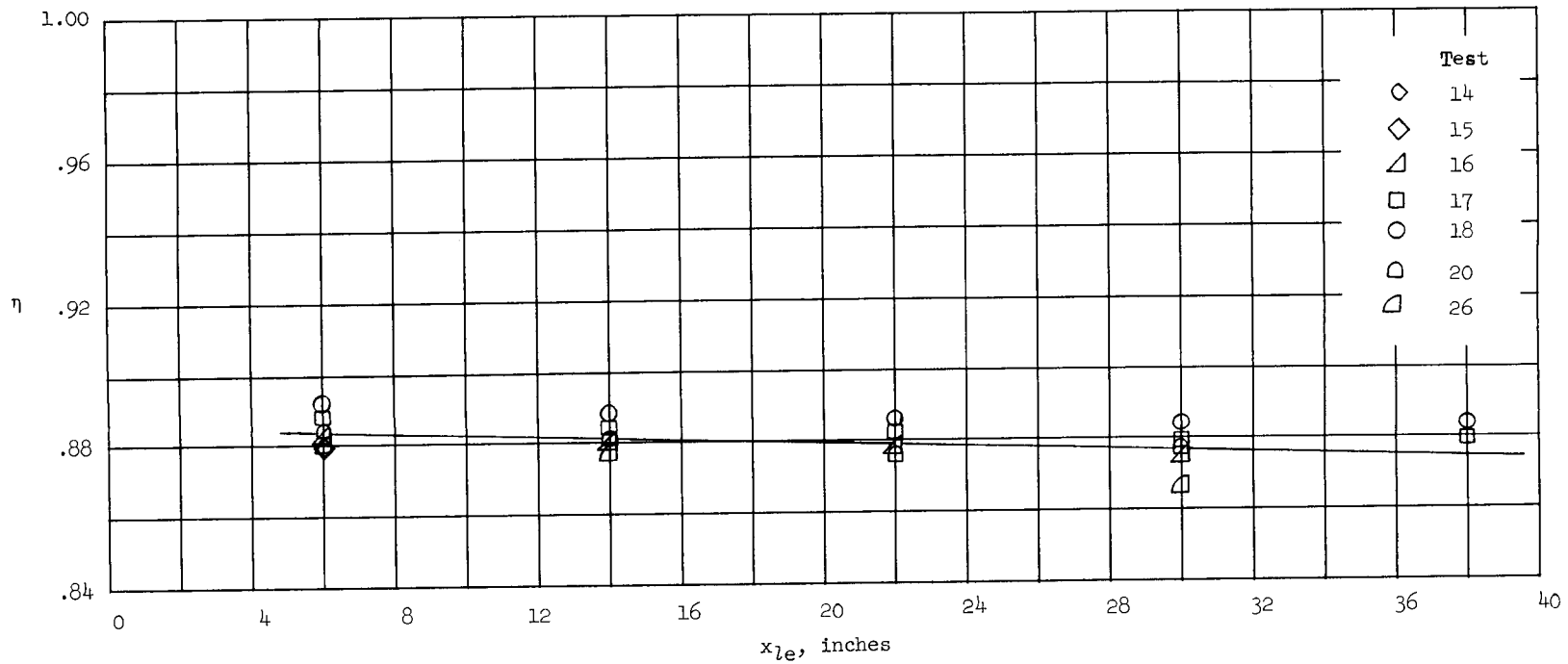

Figure 6.- Variation of turbulent recovery factor with distance from leading edge.

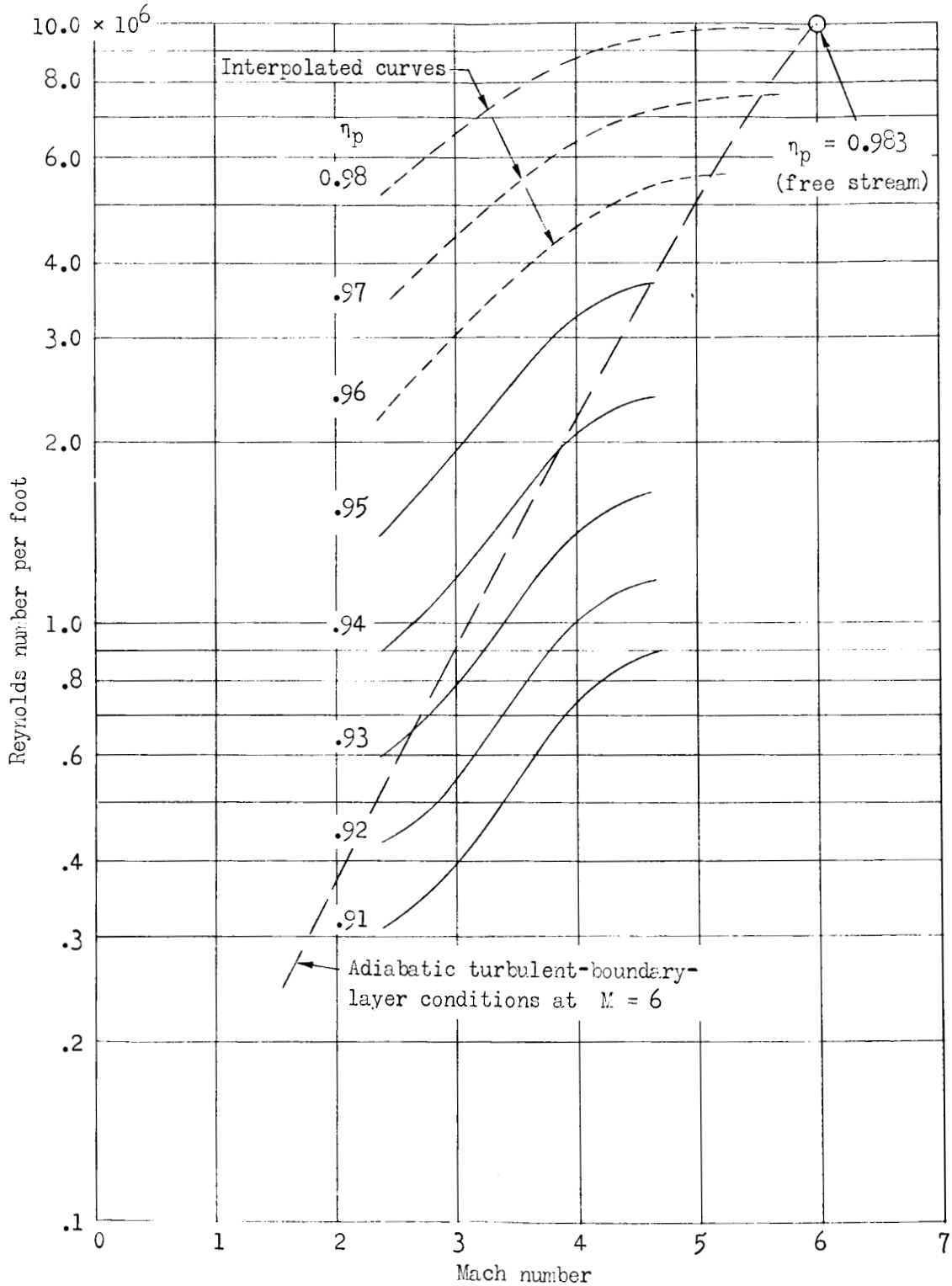

Figure 7.- Calibration plot of boundary-layer temperature probe.

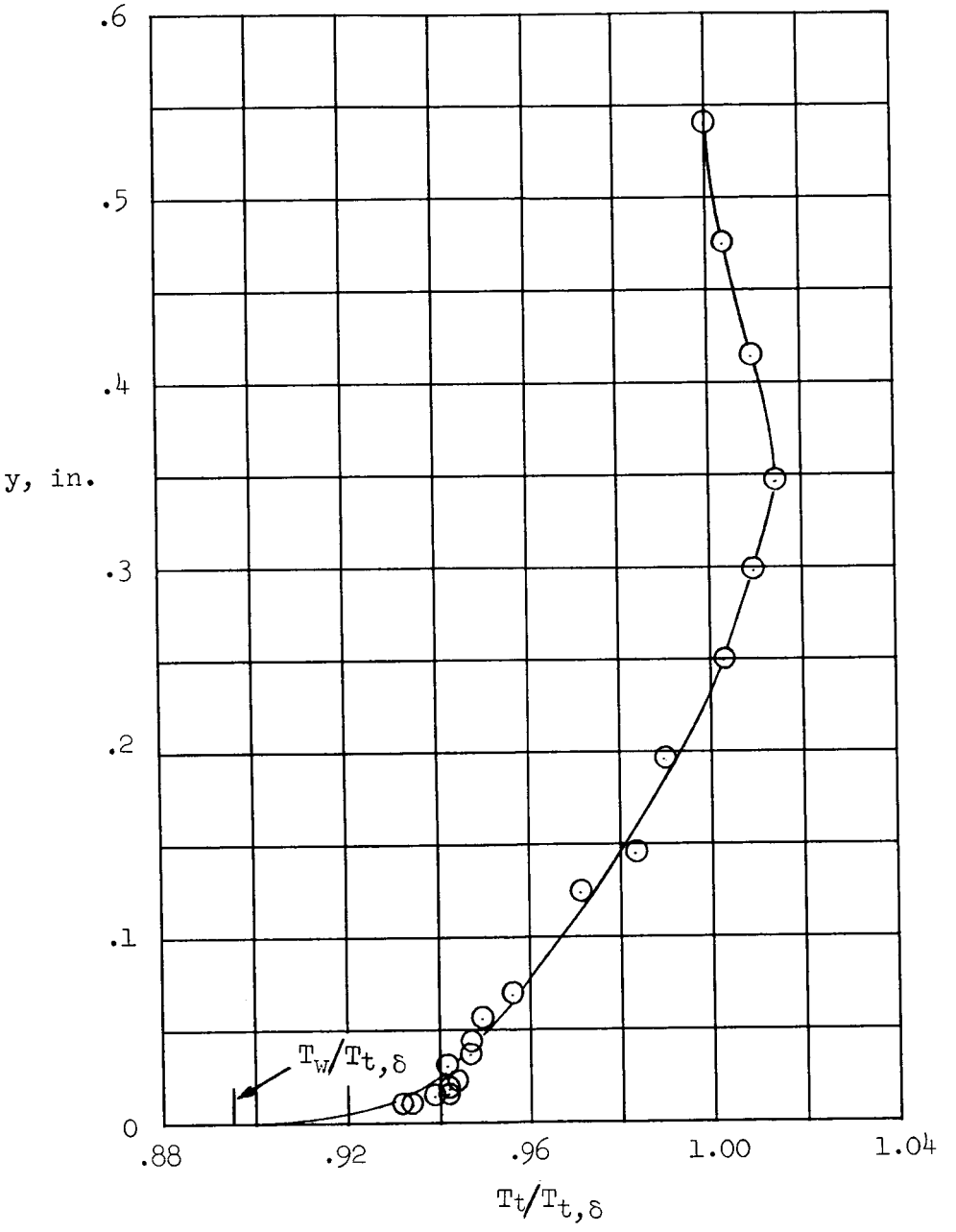

Figure 8.- Total-temperature profile at 33-inch station.

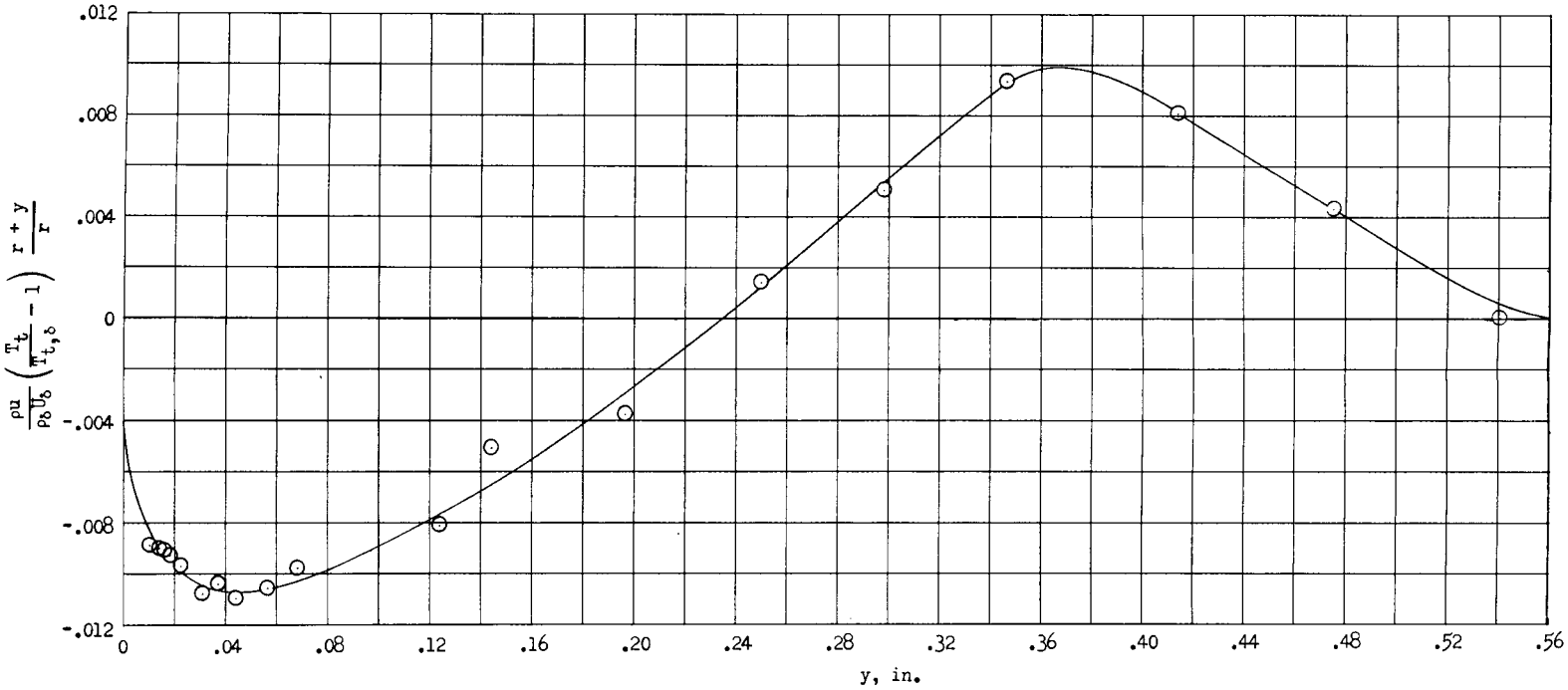

Figure 9.- Energy distribution across boundary layer at 33-inch station.

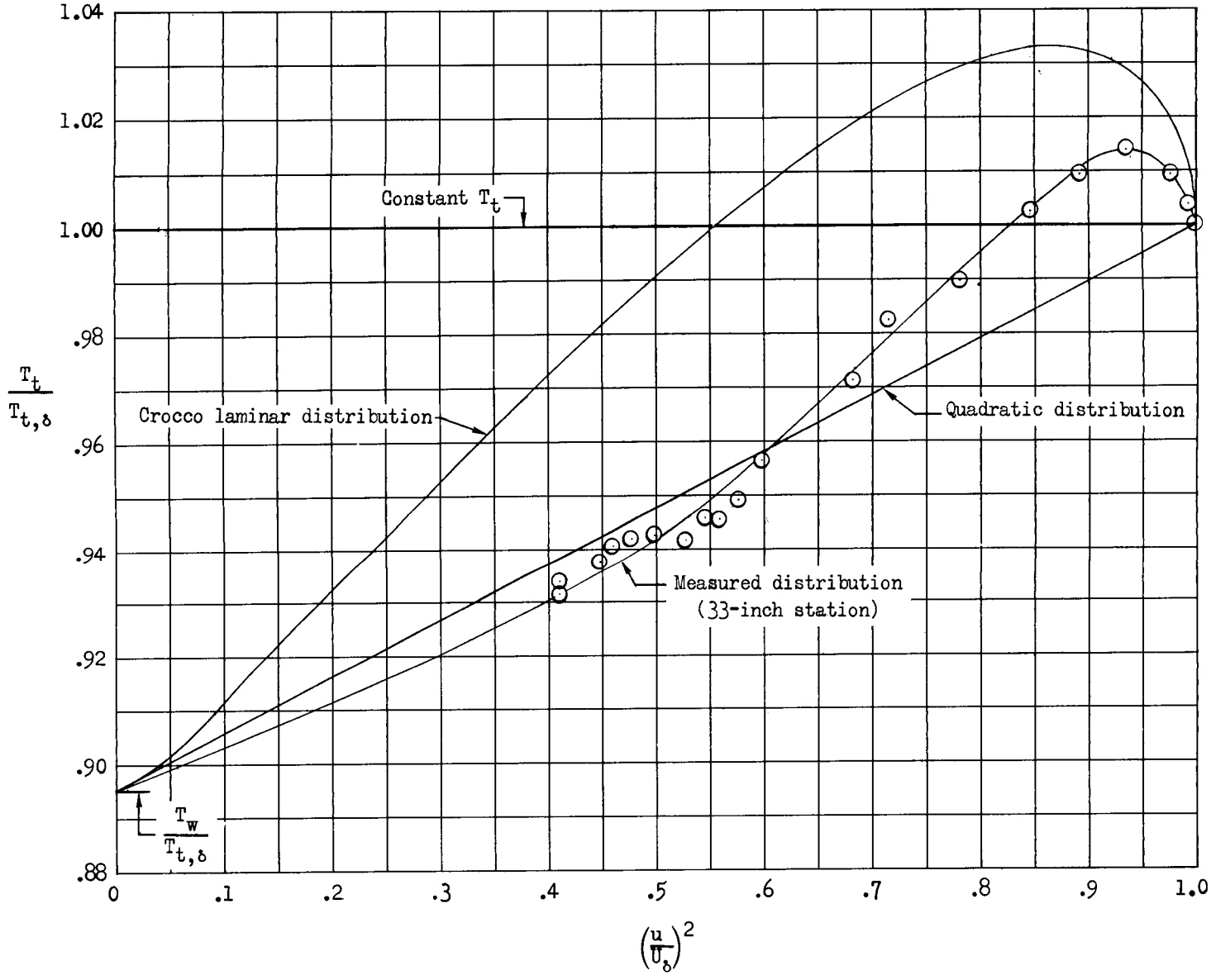

Figure 10.- Comparison of theoretical and measured variation of boundary-layer total-temperature ratio with velocity ratio squared.

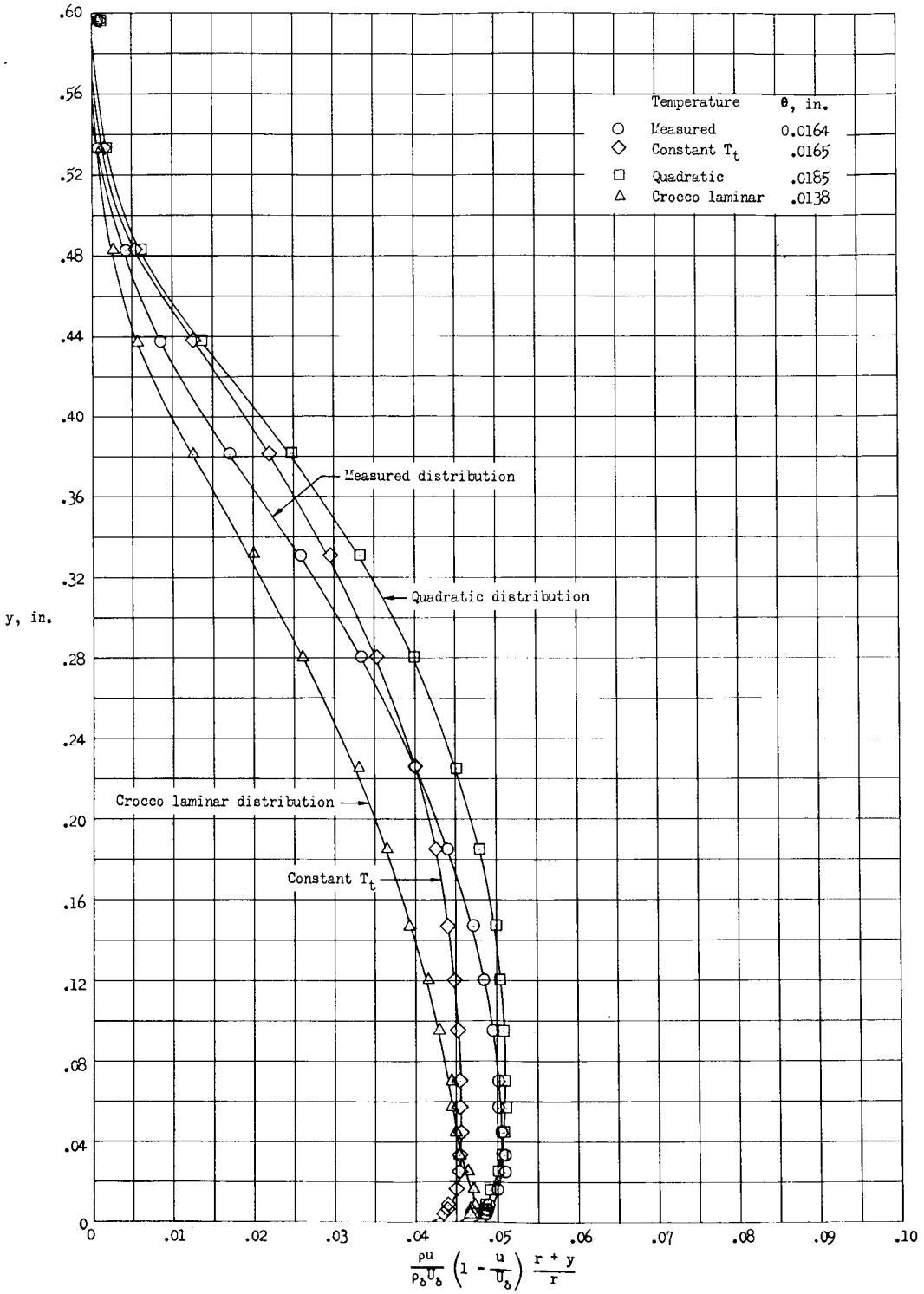

Figure 11.- Momentum profiles by various boundary-layer temperature distributions at 33-inch station.

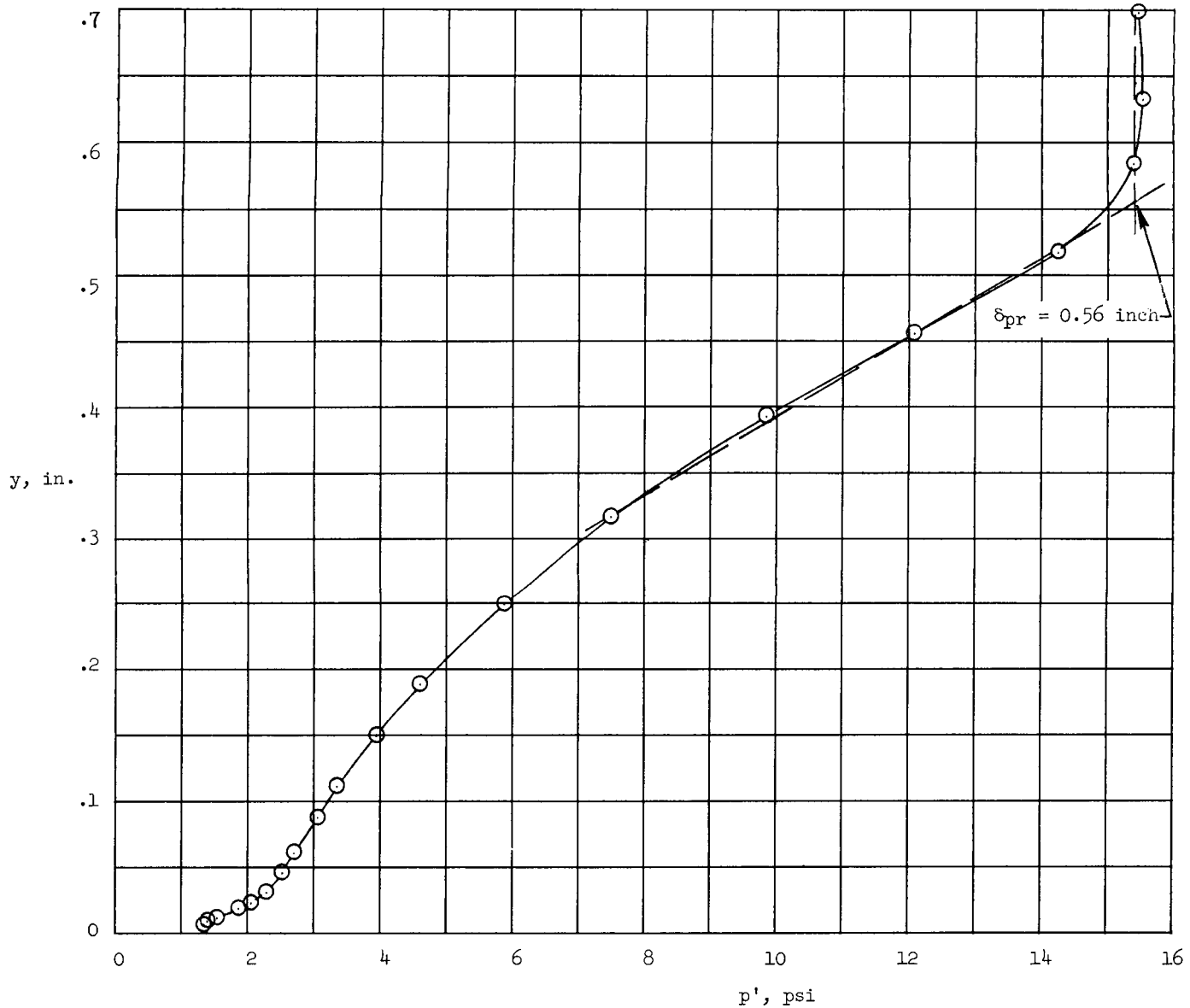

Figure 12.- Pitot-pressure distribution through boundary layer at 40-inch station.

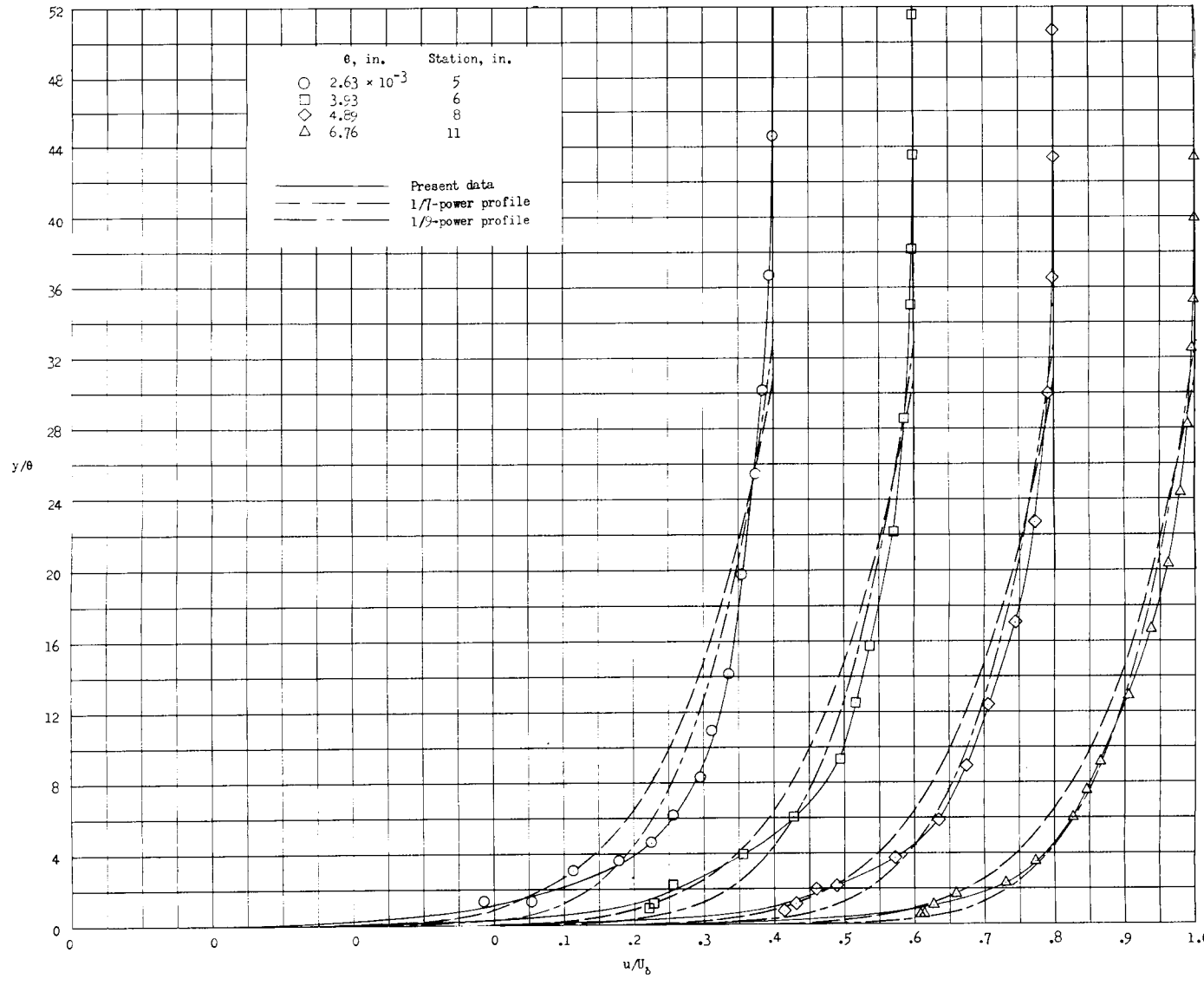

(a) 5-, 6-, 8-, and 11-inch stations.

Figure 13.- Boundary-layer velocity profiles compared with power profiles.

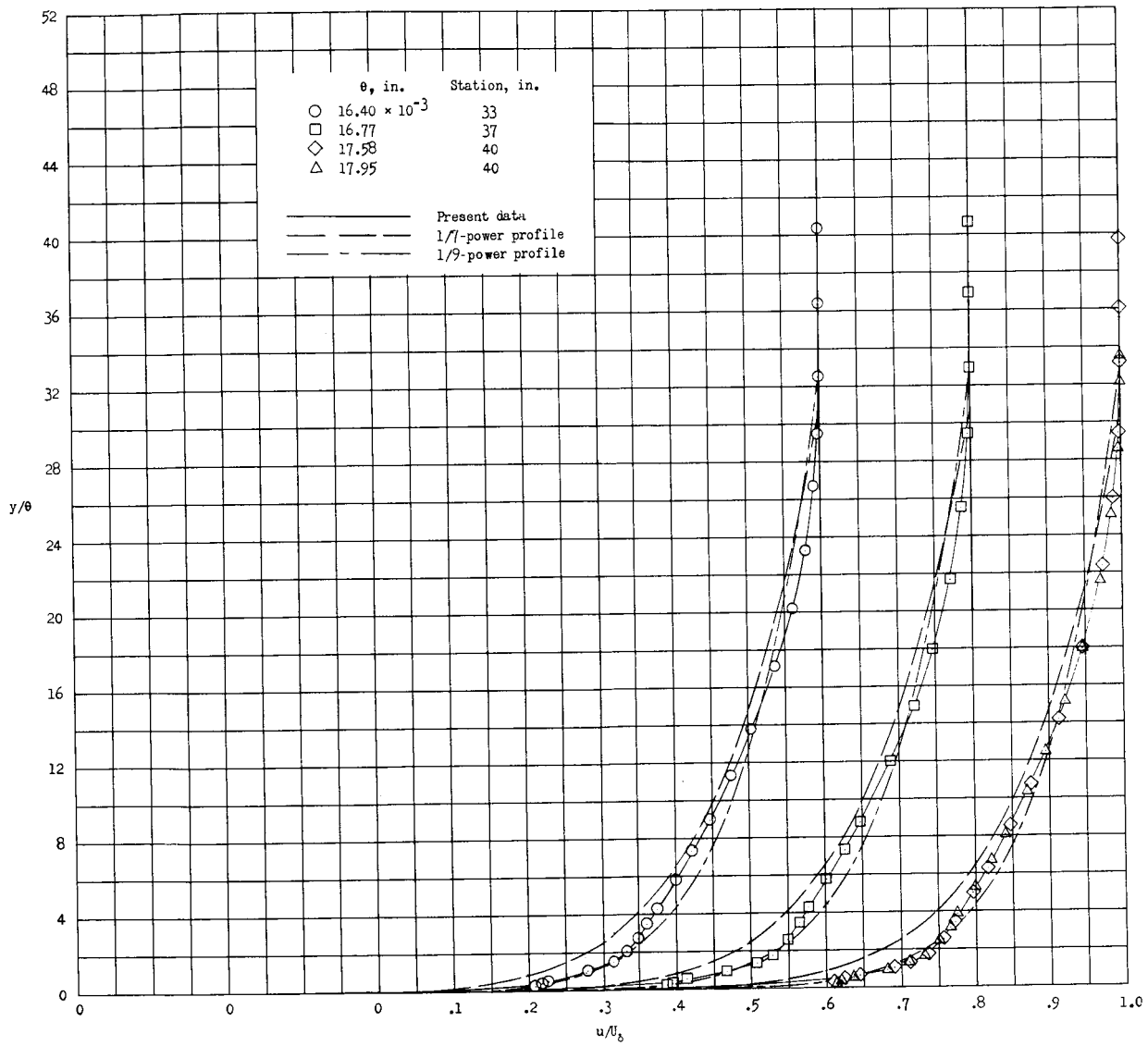

(b) 33-, 37-, and 40-inch stations.

Figure 13.- Continued.

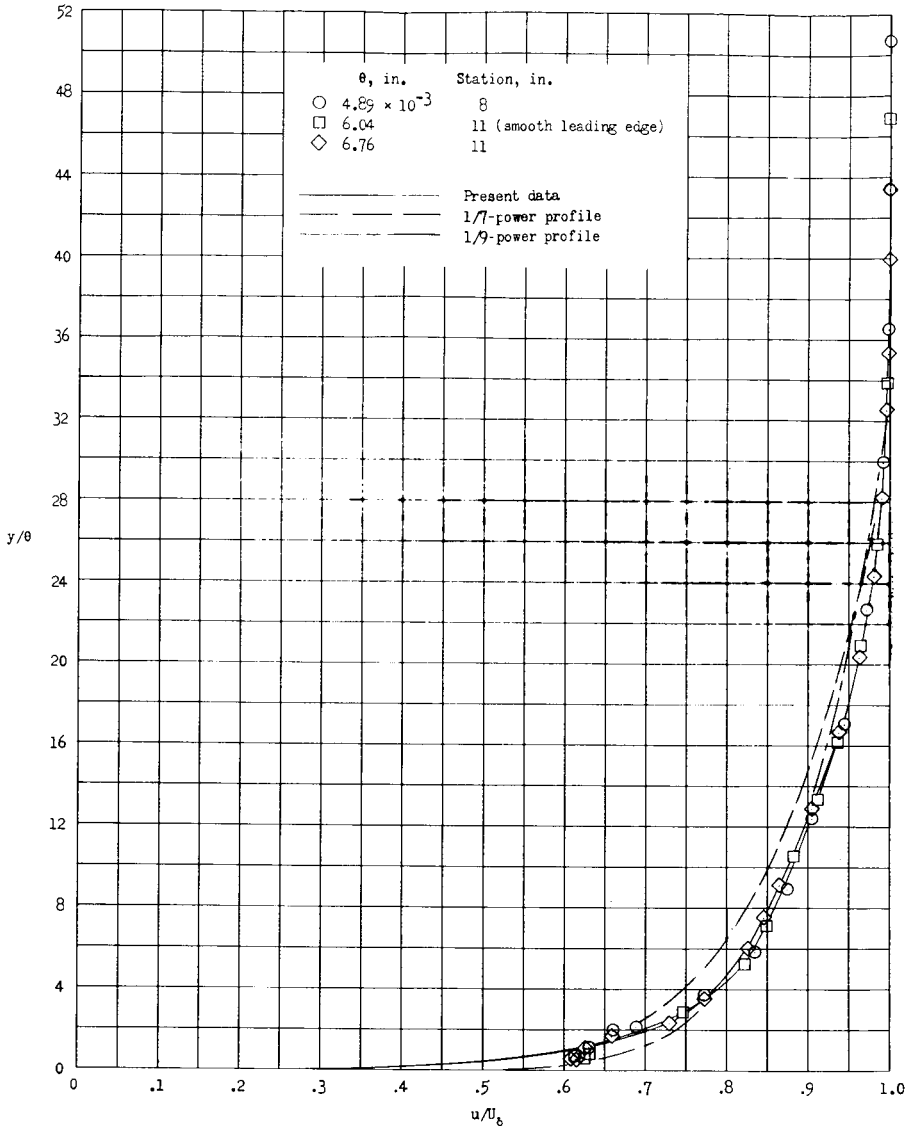

(c) 8- and 11-inch stations, including 11-inch station for smooth leading edge.

Figure 13.- Concluded.

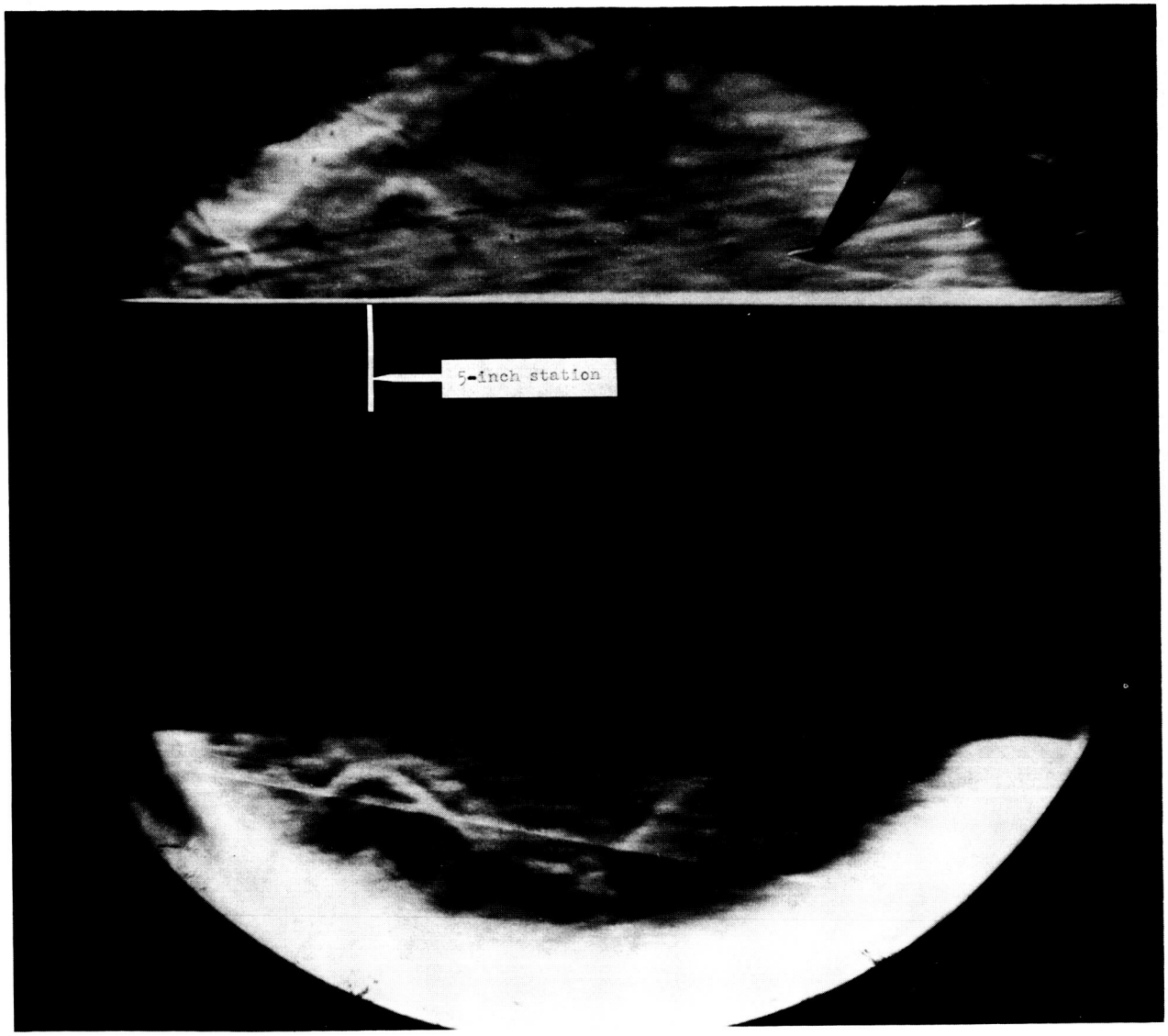

(a) Natural transition. L-65-71

Figure 14.- Schlieren photographs of boundary-layer development.

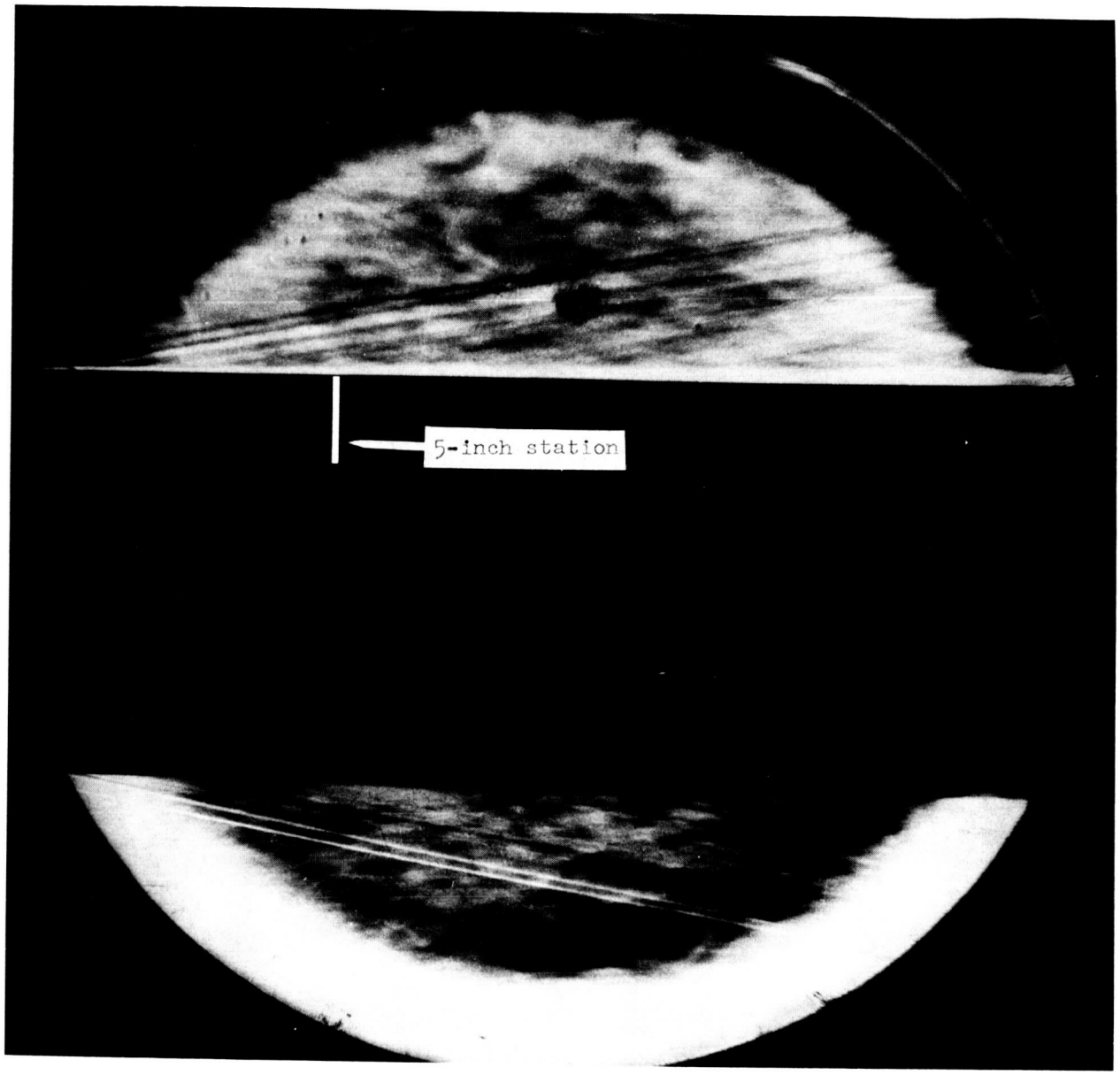

(b) Artificial transition. L-65-72

Figure 14.- Concluded.

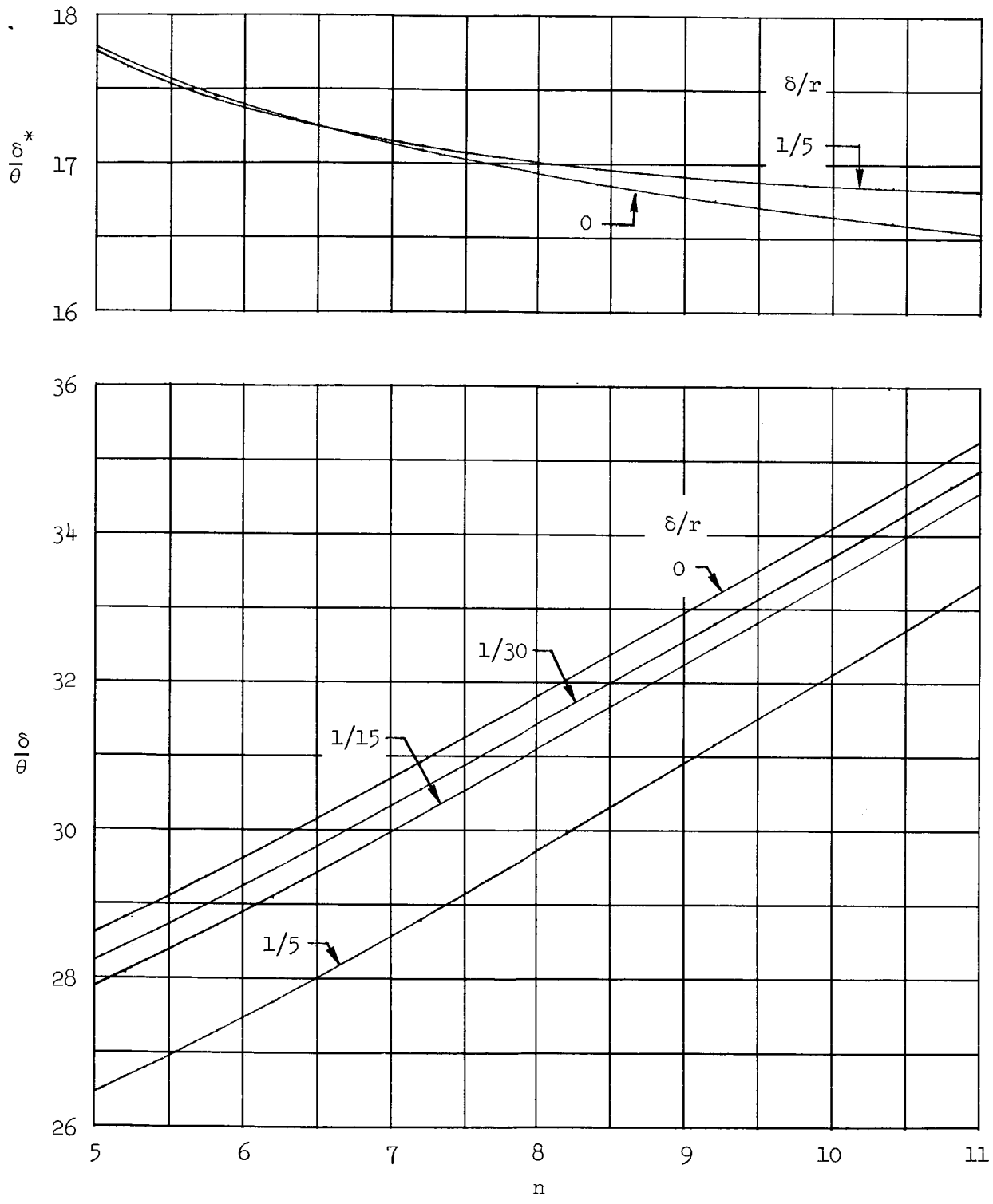

Figure 15.- Theoretical shape factors at $M = 6$ for power-velocity profiles on cylinder with total temperature constant through boundary layer.

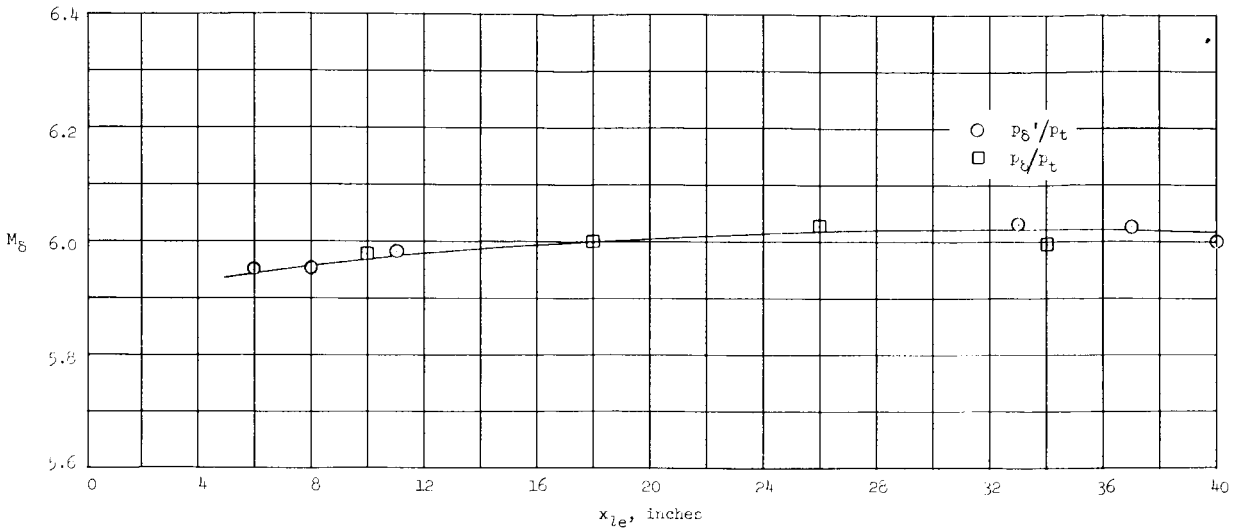

Figure 16.- Longitudinal Mach number distribution along top of cylinder.

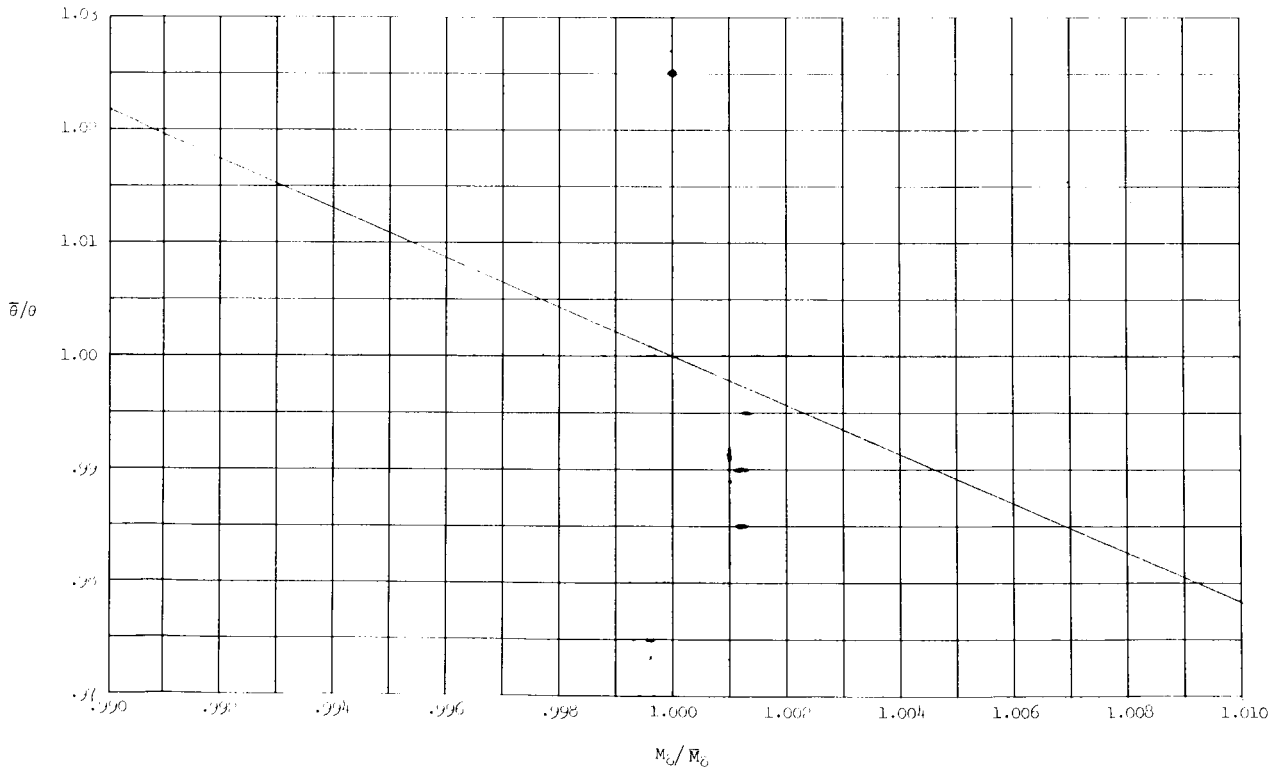

Figure 17.- Isentropic expansion from survey plane to fictitious $\bar{M}_\delta$ plane, according to Wilson (ref. 6). $\bar{M}_\delta = 5.98$.

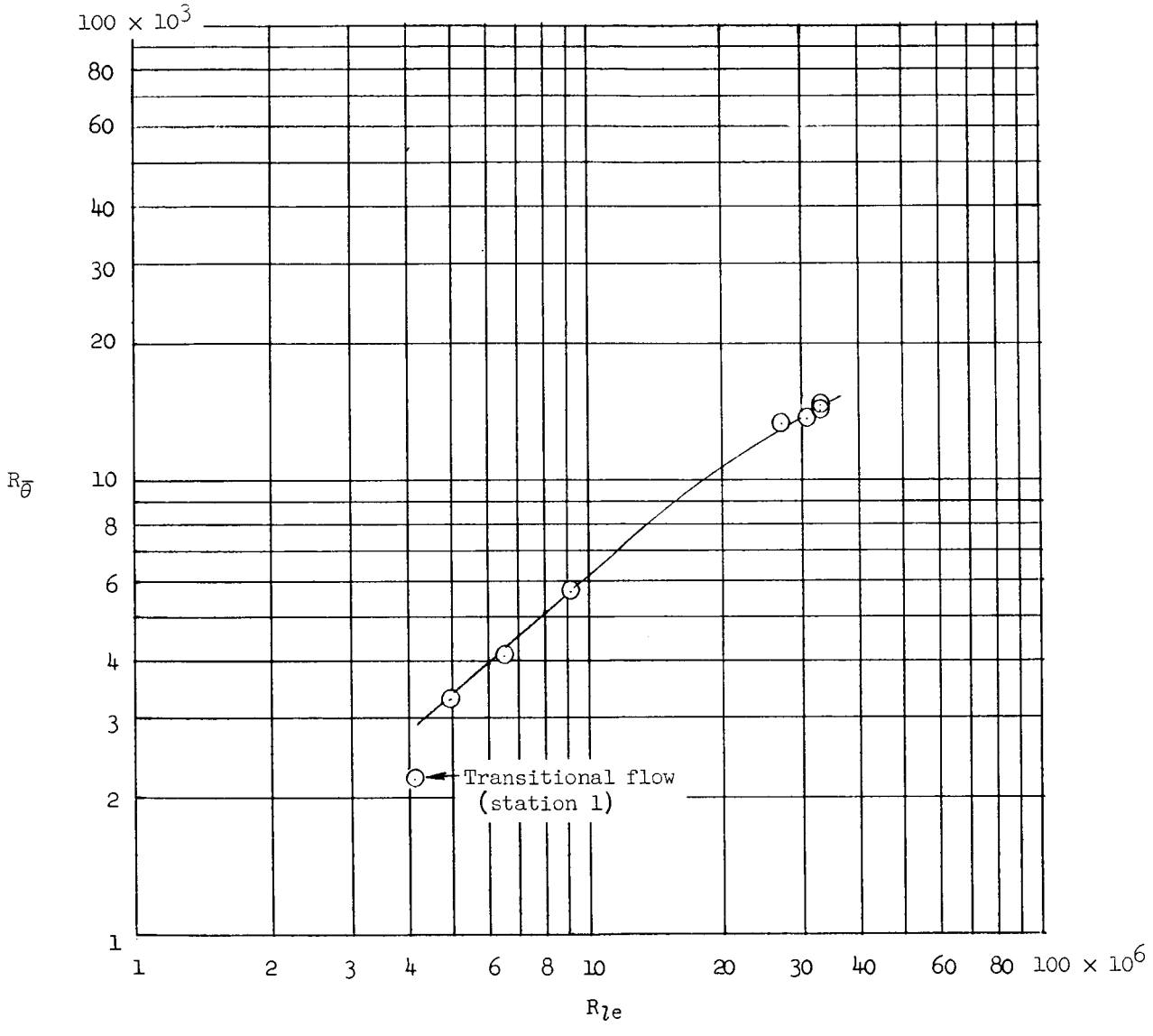

(a) Based on distance from leading edge.

Figure 18.- Variation of Reynolds number based on momentum thickness with various Reynolds numbers.

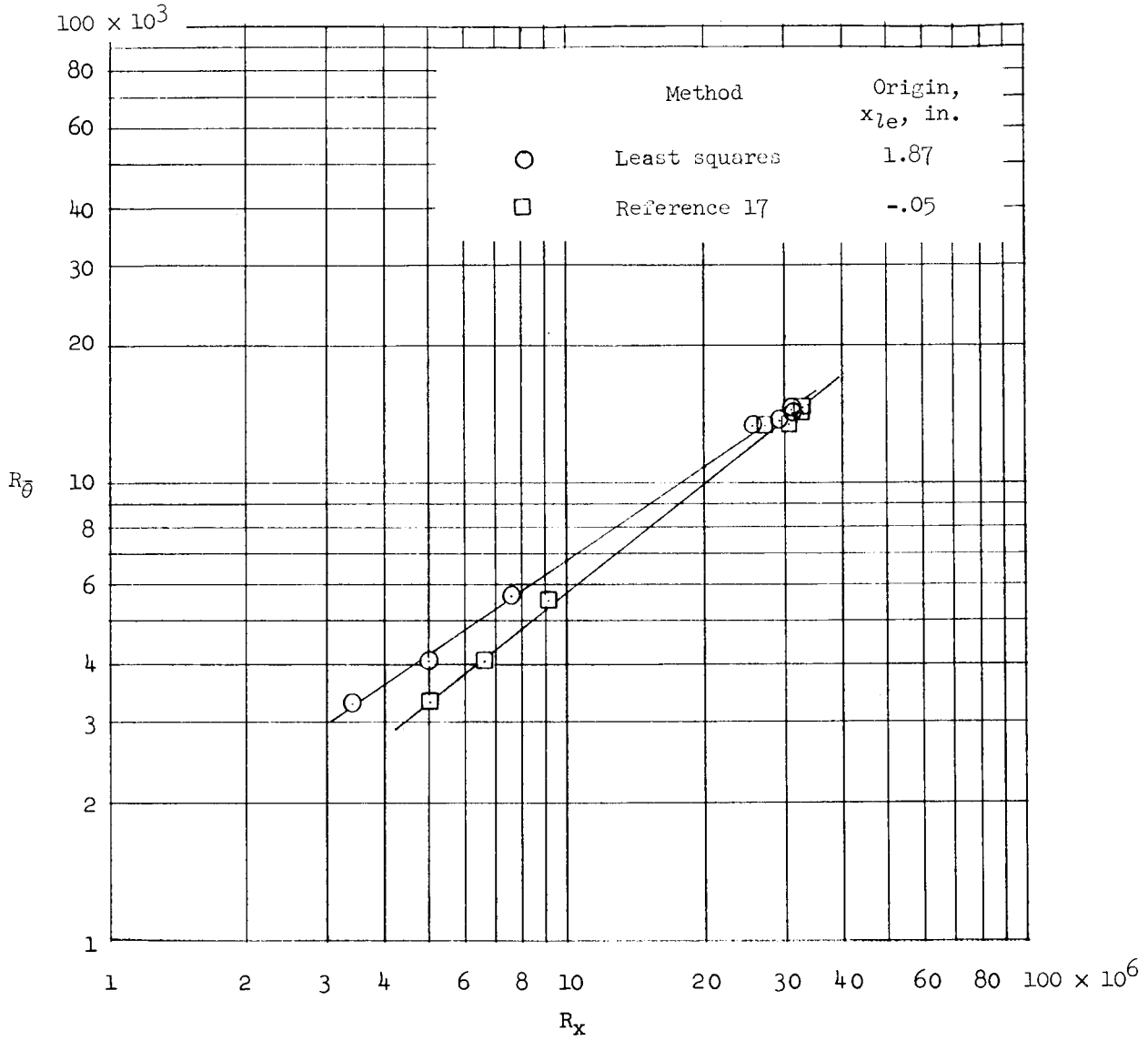

(b) Based on distance from virtual origin as found by two methods.

Figure 18.- Concluded.

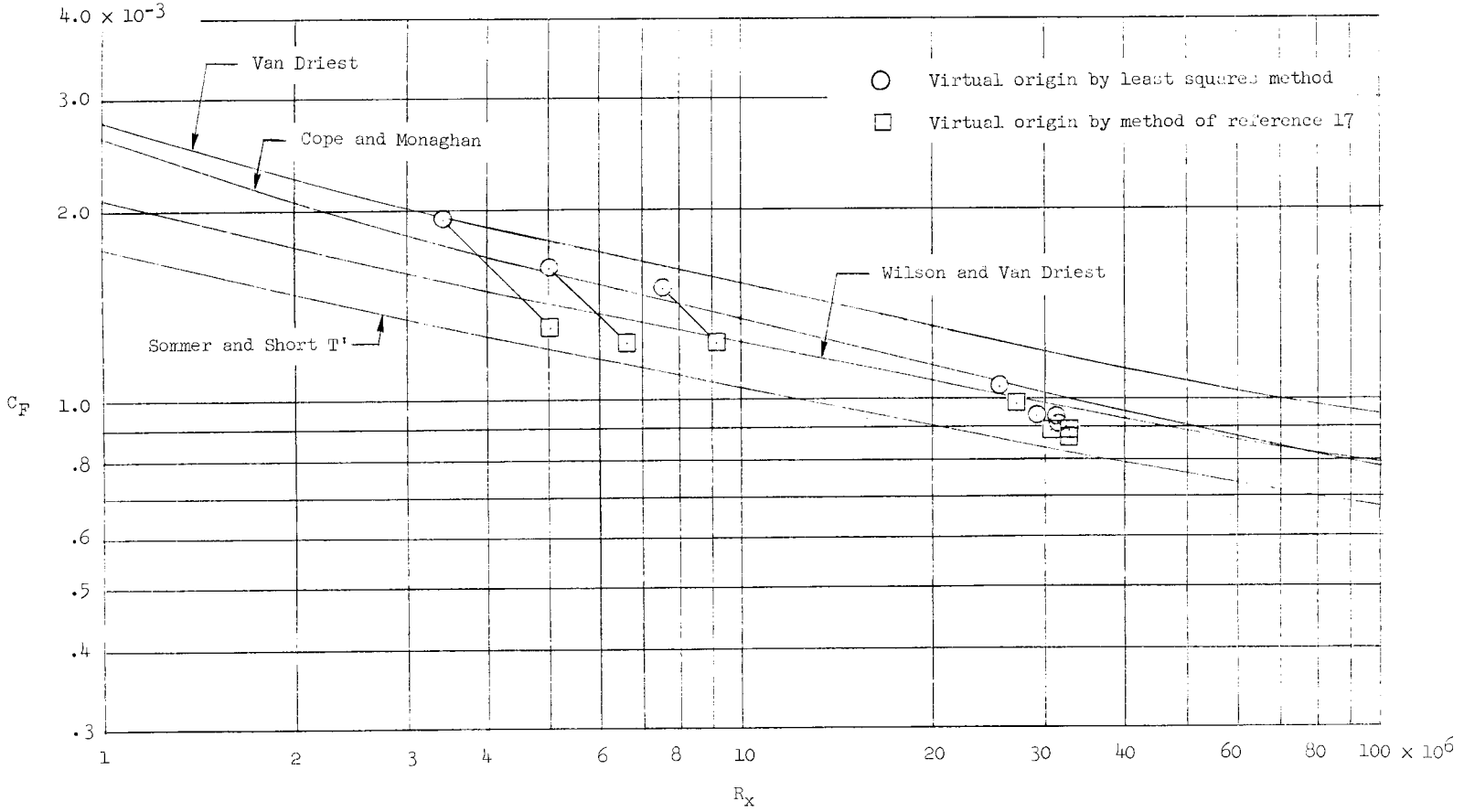

Figure 19.- Variation of average skin-friction coefficient with Reynolds number. $\bar{M}_\delta = 5.98$.

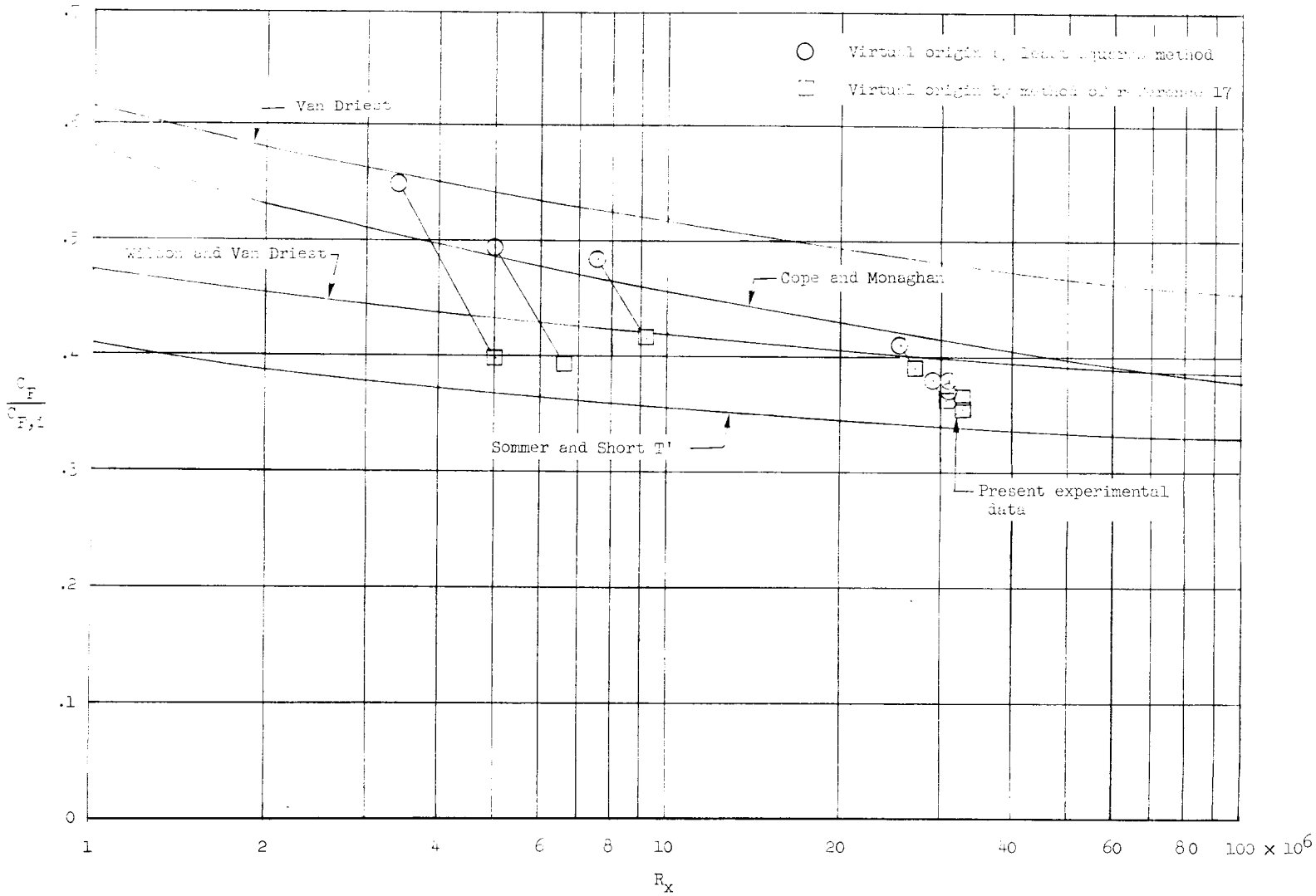

Figure 20.- Variation of ratio of average skin friction to incompressible skin friction with Reynolds number. $\bar{M}_\delta = 5.98$.

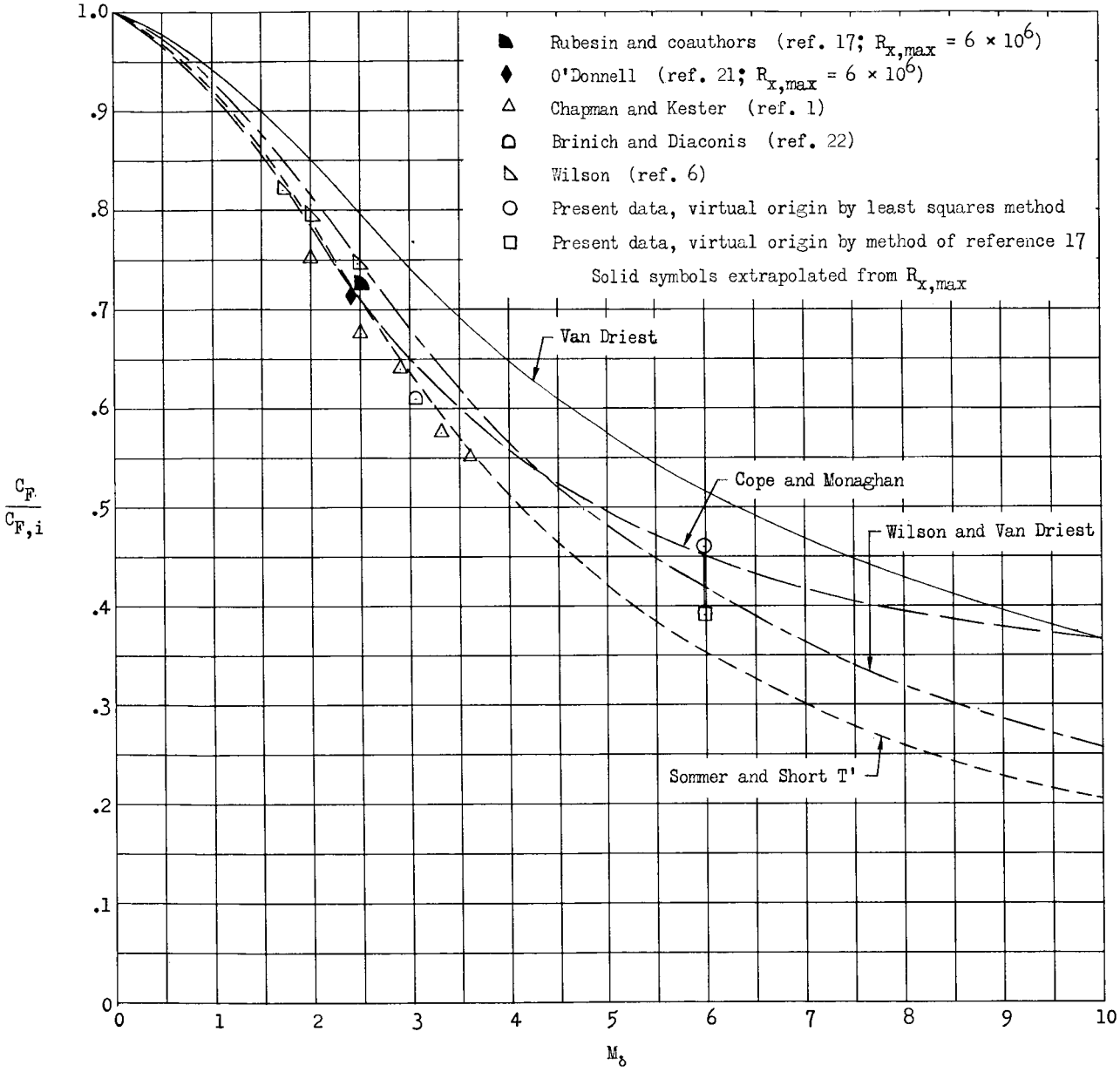

Figure 21.- Variation of various theoretical and experimental average skin-friction coefficients with Mach number. $R_x = 10 \times 10^6$.

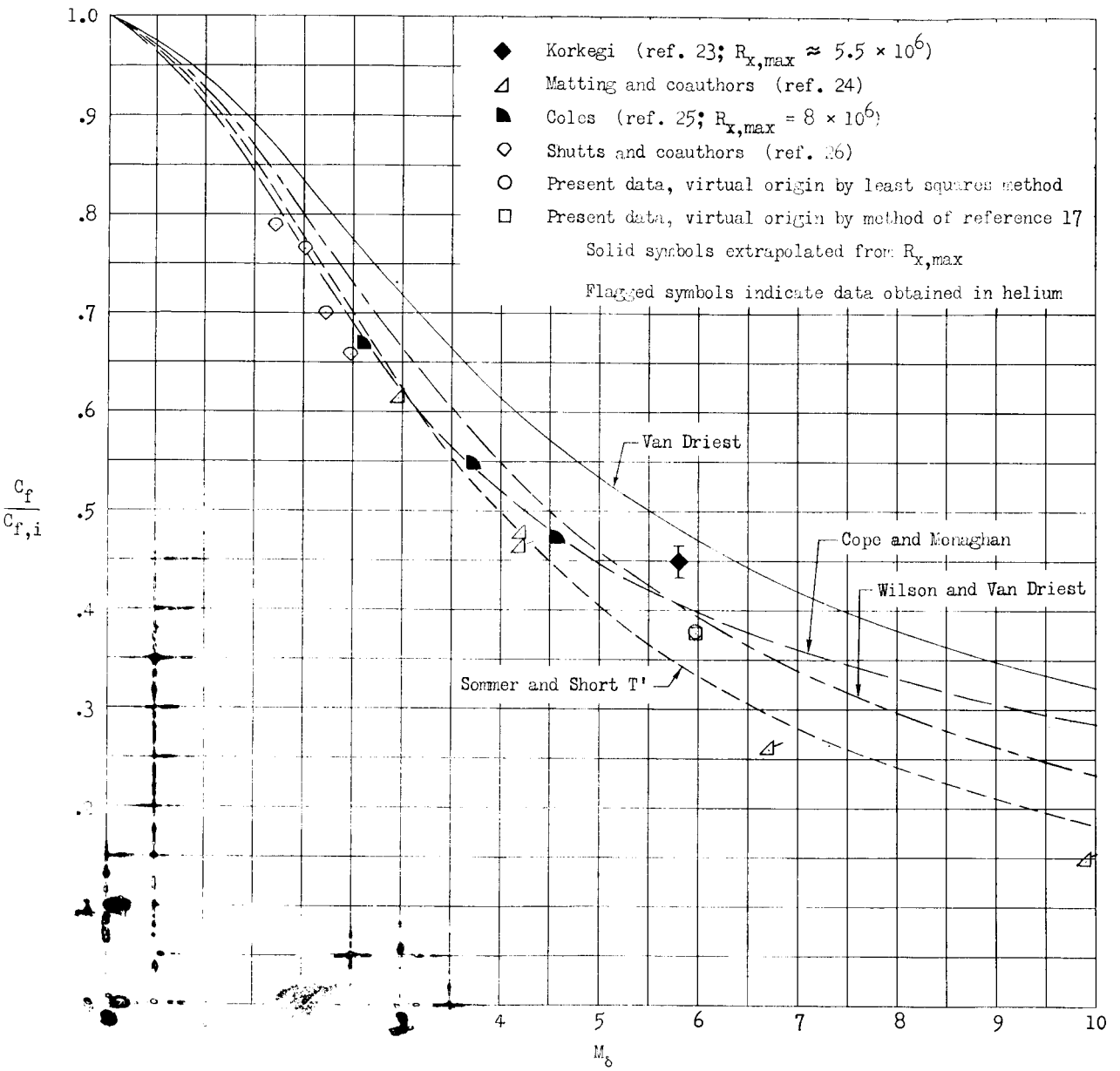

s t' oretical and experimental local skin-friction coefficients
with Mach number. $R_x = 10 \times 10^6$.

NASA-Langley, 1965 L-4035